Politecnico di Torino

Politecnico di Torino

Master's Degree in
Mechanical Engineering

April 2023

Modelling and experimental analysis of a thermal management system for a hydrogen cargo-bike

Supervisors:
Prof. Massimo Santarelli
Mohsen Mansourkiaei

Candidate:
Sergio Di Gennaro

Abstract

In the face of a decarbonization process of the transport sector to fight climate change, the usage of hydrogen for the production of mechanical or electrical energy by means of electrochemical conversion in fuel cells is becoming increasingly popular. One of the potential application of fuel cells is that of an electric cargo-bicycle (series hybrid range extender) with a battery pack, PEMFC, DC/DC converter, electric motor and electric control unit (ECU). An effective thermal management is critical for efficient and safe operation of proton exchange membrane and metal hydride, so the aims of the study are a preliminary analysis of the thermal management system by using a Simscape/Simulink model, and the testing of the system's component which are going to be mounted on the bike. The system consists of a water-cooled 300W stack, coolant circulation pump, air-water heat exchanger, and a thermally coupled metal hydride tank.

The testing phase required the organization of an acquisition system, composed by the ECU in communication with a Raspberry Pi with serial port, the electronic load and a thermal flow meter for hydrogen. Different tests are made, such as the static and dynamic characterization of the stack both with and without DC-DC converter connected, and the characterization of the thermal system. The experiments have shown the adherence of the stack to the set electrical load goals, and the cooling system capability to guarantee safe conditions during operations.

A Simscape/Simulink model is built to simulate the whole system and the hydrogen source, with a focus on the metal hydrides storage system, on the cooling system, and its control. A model validation is made by comparing the output of the simulations with the tests, showing that the model fits very well the electrical behaviour of the stack and quite well the thermal one.

Dedication

A mia madre.

Acknowledgements

Per prima cosa, sento la necessità di ringraziare tutte le persone senza le quali questo lavoro non sarebbe stato realizzato. In particolare ringrazio il professore Massimo Santarelli per l'opportunità offertami e Mohsen Mansourkiaei per l'ottimo supporto, la disponibilità e i consigli che mi ha dato. Ringrazio anche i ragazzi di Raicam, Matteo Salviani e Jean Baptiste con cui ho condiviso l'appuntamento settimanale in laboratorio e con i quali è stato un piacere e onore lavorare. Un rigraziamento speciale va a Leonardo Catalano, sempre disponibile per delucidazioni, e che è stato fonte di molti insegnamenti. Infine a Laura Gennaro va tutta la mia gratitudine per l' immenso aiuto, senza di lei questo progetto non sarebbe mai stato realizzato, ne sono certo. Nonostante questo sia stato un percorso relativamente breve, è stato per me molto formativo. Non dimenticherò facilmente il vostro aiuto e supporto. Ancora e sinceramente grazie.

Tengo a ringraziare anche i miei amici Marco, Cristiano e Andrea che mi hanno supportato e accompagnato nell'ultimo periodo. Molte persone a me care e che ugualmente ringrazio non sono menzionate, la lista è lunga, ma spero di avere in futuro occasione di poter mostrare loro la mia stima e gratitudine con gesti meno didascalici ma altrettanto sentiti.

Infine sono grato alla mia famiglia, a cui devo tutto.

Contents

Chapter 1

Introduction

Fuel cells are electrochemical devices that make use of classical red-ox reactions in order to generate electrical power. Fuel cells provide a complementary solution to heat engines, helping to reduce the widespread dependence on fossil fuels and therefore, to carry significant environmental and national security implications: "Recent studies reveal that in the United States, greenhouse gases, specifically Carbon dioxide (CO2), contribute to more than 80% of total emissions, with the transportation sector alone being responsible for 32% of CO2 emissions" [1]. To reduce our dependence on fossil fuels, we can establish a hydrogen generation and distribution infrastructure that is powered by renewable energy sources like wind, water, and solar or fuel processors. Recently, Polymer Electrolyte Membrane (PEM) fuel cell technologies have garnered global attention due to their remarkable efficiency and reduced emissions. These fuel cells employ polymer electrolyte membranes (usually Nafion), as the proton conductor and electrochemical catalysts (typically Platinum-based materials) for electrochemical reactions at low temperatures (50-100 °C). At such temperatures, both ion conductivity and charge transfer phenomena occur at a slower pace, necessitating a good catalyst to expedite the reaction rate. Despite this, the low operating temperatures facilitate quick start-up and shutdown of the cells, without requiring a prolonged time to reach or exit operating conditions. As a result, this technology is considered highly dynamic and is predominantly used in transportation applications. Moreover, PEMFC exhibits high power density, and ease of scalability.

The history of fuel cells dates back to 1839 when Sir William Robert Grove demonstrated the first fuel cell by using platinized platinum electrodes

in dilute sulfuric acid to show that the electrochemical dissociation of water was nearly reversible. Another significant milestone was the development of the first practical fuel cell by General Electric Company (GE) in 1962 for the Gemini space mission. In the 1960s, improvements were made by incorporating Teflon in the catalyst layer directly adjacent to the electrolyte, and significant advancements were made in the 1970s with the adoption of the fully fluorinated Nafion membrane. Until a few decades ago, PEM fuel cells did not receive much attention. However, breakthrough methods for reducing the Pt loading required for PEM fuel cells were developed and improved. In 2017, Toyota launched its first commercial fuel cell vehicle, Mirai. Despite many breakthroughs, challenges such as reducing cost and improving durability remain before the widespread deployment of PEM fuel cells [2].

Fuel cells have several advantages over internal combustion engines (ICE) and batteries. To generate mechanical energy, the ICE first converts fuel energy to thermal energy by combusting fuel with oxygen at high temperature. But the conversion of thermal energy to mechanical energy in ICE is limited by the Carnot Cycle. Fuel cells, on the other hand, directly convert fuel energy to electrical energy and are not limited by Carnot Cycle constraints. As a result, fuel cells have the potential to achieve higher energy conversion efficiency than internal combustion engines (ICE). When hydrogen is used as fuel, the reaction in fuel cells produces only water and heat, making them a zero-emission power generator that does not emit pollutants such as hydrocarbons or nitrogen oxides. Moreover, in contrast to batteries, fuel cell reactants are stored externally in high-pressure, cryogenic or metal hydrides tanks that can be refueled quickly, whereas batteries store reactants internally and must be recharged or replaced when used up [3]. The power response of the fuel cell system is determined by factors such as the regulation of air and hydrogen flow and pressure, as well as heat and water management. When current is drawn from the load source connected to the fuel cell stack, heat and water are generated, and oxygen is depleted.

1.1 Proton-exchange membrane fuel cell

In a PEM fuel cell two electrodes are separated by a polymeric membrane that does not conduct electrons but lets the positive ions pass. In this way

an electric current is produced by the fuel cell. The semi-reactions are:

$$H_2 \longrightarrow 2\,e^- + 2\,H^+$$

$$2\,H^+ + 2\,e^- + \frac{1}{2}\,O_2 \longrightarrow H_2O$$

The movement of H^+ ions from the negatively charged anode to the positively charged cathode occurs through an electrolyte that contains H^+ ions in the fuel cell, which is referred to as a Cationic Electrolyte. The electrodes' major concentration of catalyst is located close to the membrane to facilitate red-ox semi-reactions near the electrolyte. As a result, protons have to travel a shorter distance to pass from the anode to the cathode. The layers responsible for catalyzing reactions in the fuel cell are known as catalyst layers. On the other hand, the portions of the electrode between the membrane and the interconnectors, where hydrogen and oxygen sources pass through, are referred to as diffusion layers. These layers allow only the diffusion of reactants towards the catalyst layers. The interconnectors also enable the transfer of e^- from the anode to the cathode of two different yet adjacent cells in the same stack. Electrons are unable to cross the electrolyte layer and must instead move from the anode to the cathode of two separate cells separated by bipolar interconnectors (typically constructed from graphite). In contrast, protons H^+ travel from the anode to the cathode via the membrane inside the same cell, and consequently, move in the opposite direction to the flux of electrons. The electric energy production depends on the different pathway of reactants (protons and electrons) in semi-reactions, and therefore, protons cannot follow the same route as electrons through an interconnector. Consequently, the interconnector material must have a low ion conductivity. The fundamental role of the interconnector and the organization in the structure assembly of the stack leads to the identification of a so-called SINGLE REPEATING UNIT composed by:

1. Interconnector
2. Anode
3. Electrolyte
4. Cathode

In this order. The repetition in series of this unit build up the PEMFC stack. The part of an SRU composed by the only cell takes the name Membrane Electrode Assembly (MEA). The water produced as waste (product) of the combustion reaction is collected in a pipe that runs parallel to air excess pipe.

The polymer of the electrolyte contains transverse chains that terminate with a HSO_3 (hydrogen sulphite) group, which contains a weak bond between the sulphite group SO_3 and the hydrogen H that is readily broken and regenerated. This weak bond is responsible for the migration and transportation of the proton H^+ from the anode to the cathode. Consequently, the H^+ moves gradually, via jumps, from the chains in contact with the anode towards those in contact with the cathode (the direction of movement is determined by the concentration gradient of protons generated by semi-reactions at the anode and cathode). Importantly, the migration of the proton from one bond with a chain to the next sulphite group and the breaking and formation of the bond can only occur if the proton is a hydrated ion. This indicates that in order for the H^+ ion to be transported, it must be part of a complex with a positive charge, composed of one or more water molecules and the proton itself. The requirement of liquid water for the humidification of NAFION is essential and unique to PEMFC, and has various direct or indirect effects that significantly define PEMFC systems:

1. Necessity to maintain humidified the membrane;
2. Necessity to operate at $T < T_{H2O.eva}$;
3. Charge transfer in the electrode has to be improved by catalyst of high quality such as Pt, Ir, Ru, Pd;
4. No carbon fuels are good for PEMFC. This is because Pt suffers poisoning from C-containing molecules;
5. Because of the 4^{th} effect the necessity to feed the anode with only ultra pure H_2 as fuel.

The highest ΔV recorded is the Open Circuit Voltage, which pertains to a cell that has an open conductor preventing the flow of electricity. The voltage produced by a fuel cell can range from 0 to 1 Volts, depending on the fuel cell's operating conditions and the size of the load it is connected to. Generally, a single fuel cell generates an average voltage of 0.7 Volts. A

"Polarization Plan" graph is a tool used to analyze the performance of a fuel cell in a closed circuit by plotting the correlation between the current and voltage. Three types of over-voltage can occur in the cell:

- Activation over-voltage. It refers to the amount of energy required to break the equilibrium, which is taken from the electrochemical potential available in the cell, resulting in a voltage drop;
- Ohmic over-voltage. It is caused by the passage of charge, generating ohmic effects (joule effect). During the pathway, the charges collide with the atom, delivering energy in the form of heat. The main effect of the voltage drop due to the joule effect is generated by ions migrating from the anode to the cathode through the electrolyte; [4]
- Diffusion over-voltage. It is exhibited in the case of high current values, when the diffusion of the reactants is not fast enough to satisfy the request of charges from the cell.

1.2 PEMFC in light mobility and cargo-bike

Traditional bicycles remain the most efficient and environmentally friendly mode of transportation worldwide. However, electric bikes are becoming increasingly popular due to their ability to compensate for physical exertion during long-distance rides, adapt to changes in road geometry, and use satellite communication systems. Hydrogen fuel cells have also demonstrated great potential as a low-emission and efficient power source for bicycles when used in hybrid powertrains with an energy storage system, as sudden oscillations in the vehicle's demand cannot be met by a Full-FC powertrain alone [5]. An e-Bike operates similarly to a traditional bike, but with the added benefit of an electric motor that provides assistance to the rider. This assistance can be adjusted to various levels, from a gentle nudge to a strong push, which is particularly useful for e-Cargo bikes that transport heavy loads over long distances. Sensing systems are used to detect the rider's pedal movements and generate a signal to the motor to provide assistance based on the amount of torque being generated.

1.3 Metal hydrides tank

One of the obstacles to the widespread adoption and commercialization of hydrogen is its storage issue. To use hydrogen as a fuel source for vehicles, it must be stored in a compact manner, and the weight of the storage equipment such as the container, heat transfer apparatus, and other components should be minimal to make it a feasible alternative fuel. "The United States Department of Energy (DOE) has published a set of targets that focus on the system-level performance of any storage system". This allows for more transparent comparisons between storage systems by considering their system-level characteristics. Some of the issues that arise when considering materials based storage are:

1. Is it possible to recharge the material on-board the vehicle, or is off-board recharging at a central plant necessary? If off-board recharging is required, how will the material be transported to and from the vehicle at the refueling station? Additionally, is the off-board regeneration process both efficient and cost-effective?

2. Is the process of hydrogen release exothermic or endothermic? Additionally, does the rate of the reaction occur quickly enough to facilitate the necessary dynamic rate for accepting and releasing hydrogen?

3. What is the required temperature range for the material to function properly?

In cases where the material is cryogenic, such as with adsorbent materials, there may be issues with dormancy. On the other hand, if the operating temperature is lower than that of the fuel cell, the waste heat generated by the fuel cell stack can be utilized for de-hydrogenation. However, if the required temperature is higher than that of the fuel cell, then the waste heat will not be available for the endothermic process of hydrogen release. [6]

Hydrogen can be stored through compression, liquefaction, or by binding it to a substance that can release the gas in a nearly reversible way. However, compression requires extremely high pressures, ranging from 350 to 700 bar or more, which demands significant amounts of work. In contrast, liquefaction can achieve high gravimetric densities at lower pressures, but it is even more costly than compression due to the need for electrical power to cool the hydrogen to extremely low temperatures (around 20 K at 1 bar).

Although these storage methods are currently used for on-board hydrogen vehicles, they fail to meet all the targets set by the DOE, and researchers are actively exploring other options. Among these options, the storage of hydrogen on solid materials is being evaluated and studied by many scientists and researchers. Storing hydrogen using a media is advantageous because it allows for storage at lower pressures compared to compressed hydrogen, and also requires much less electric power than liquefaction which results in higher volumetric density and improved safety compared to traditional methods. Media used for vehicular hydrogen storage is conventionally divided into three classes:

1. Chemical hydrides which can be refueled off board a vehicle;

2. Adsorbents, which need to be maintained at low temperatures to store a sufficient amount of hydrogen. They can also be refueled on board a vehicle (Physisorption);

3. Metal hydrides that undergo chemical reactions when charged and discharged, and can be refueled on board.

The charging and discharging of hydrogen is a complicated process that involves the interaction of chemical kinetics or thermodynamics with mass, momentum, and thermal transport processes. Solid storage methods, similar to physical storage methods, have drawbacks when it comes to their use in the automotive field. Physisorption systems, although not needing temperatures as low as liquid hydrogen, still require cryogenic temperatures close to that of liquid nitrogen (77 K) to store enough hydrogen for current vehicle needs. Chemisorption systems can be classified into two types of materials: reversible and non-reversible systems. Regarding their use in automobiles, non-reversible systems are those that rely on materials which cannot be easily recharged with gaseous hydrogen at a fueling station. These systems, known as chemical hydride systems, require off-board recharging which involves more complex processing conditions to successfully rehydrogenate the material [7]. On the other hand, reversible materials are a class of materials that can usually be recharged with hydrogen under conditions that are typically present at some of today's gaseous or liquid refueling hydrogen stations. These systems are commonly referred to as metal hydride systems. Metal Hydride (MH) systems involve an exothermic desorption reaction that releases heat. For the past three decades, reversible metal hydrides have been

assessed for vehicle applications, the majority of these systems have utilized intermetallic alloys (such as TiCrMn, $LaNi_5$, and FeTi) or pure metals like Mg [8]. Typically, the heat generated by a PEMFC is dissipated to the ambient, while an external heat source is used to heat the Metal Hydride Tank. This approach reduces the efficiency of the overall PEMFC system. However, it is possible to extract usable hydrogen (H2) by recycling the heat generated by the PEMFC and injecting it back into the MHT [9].

1.4 Thermal management

Efficient cooling plays a vital role in the secure and productive functioning of fuel PEMFC stacks. Even though PEMFCs exhibit high efficiency in energy conversion, a considerable amount of heat is still produced during operation. To prevent components, especially the membrane, from overheating, it is crucial to remove the generated heat efficiently. Management of the temperature of the fuel cell stack is more complex than that of an internal combustion engine. It is due to two reasons: firstly, the stack uses de-ionized water as a coolant instead of an efficient coolant fluid. Secondly, the narrow range of operating temperatures and small temperature differences between the stack and the surroundings make designing a cooling system significantly challenging. The objective of thermal management is to achieve fast warm-up without overshooting the stack temperature and consuming low auxiliary power. PEMFCs used today typically operate most effectively within a temperature range of 60 to 80 °C. When temperatures exceed this range, it can cause a more rapid breakdown of the membrane and catalyst, which can result in decreased performance of the stack. Conversely, lower temperatures can negatively impact reaction kinetics and lead to flooding, a significant issue from a water management standpoint, due to the lower water saturation pressures at lower temperatures [10]. Besides the difficulties in removing heat, the parasitic power consumption, volume, and mass of the stack can be affected by the cooling methods and cooling system designs utilized. To maintain the safe and stable output performance of the PEMFC, and prevent thermal runaway, thermal management components, i.e. a coolant circulation pump and radiator fan, have to be coordinated. Different cooling strategies can be applied, such as:

- Cooling with heat spreaders. It involves the conduction of heat in the same plane as the cooling plates to transfer heat from the central region

to the edges of the PEMFC stack. This edge cooling approach eliminates the need for coolant circulation within the stack, reducing the weight and complexity of the cooling system while enhancing the overall system's reliability compared to traditional liquid cooling methods. However, one significant challenge of cooling with heat spreaders is the need for high in-plane thermal conductivity of the cooling plates to ensure consistent temperature control across the active area. The two primary methods for achieving this are using materials with high thermal conductivity and implementing heat pipes. While this approach simplifies the stack, it does have limitations on heat transfer.

- Cooling with separate air flow. It involves the creation of cooling channels within the bipolar plates or using separate cooling plates placed between them. This approach is generally appropriate for PEMFC stacks with power outputs ranging from 100 W to 2 kW. However, for stacks with power outputs exceeding 5 kW, air cooling may not be sufficient or as beneficial as liquid cooling.

- Cooling with phase change. Coolant is water or another phase-change medium.

- Liquid cooling. The coolant used in a PEMFC system can either be deionized water or antifreeze coolant, and cooling is implemented between each cell or each pair of cells. In a water-cooled PEMFC system, the temperature of the coolant is a critical control parameter that impacts the transfer of gases, water balance, and electrochemical reaction activity, ultimately affecting the performance of the fuel cell. Operating the system at a higher temperature can enhance the electrocatalytic activity, leading to better output performance. However, maintaining water balance becomes more challenging in systems operating at higher temperatures [11] [12].

Cooling methods depend on several factors, such as the size of the FC, the complexity of the system, the application, the cost and the amount of heat recovered. Each cooling strategy has its own advantages, limitations and challenges.

Chapter 2

Literature review

Over the past three decades, various models for fuel cells have been introduced in literature. The majority of research on PEM fuel cell modeling has focused on examining the electrochemical, diffusion processes and parameters optimization of individual fuel cells, unit cells or specific elements of the unit cell. Significant examples include the work of M. Secanell et al [13], where a numerical model for designing the cathode electrode is introduced and utilized to anticipate the optimal electrode performance at varying operational conditions, and the work of Zhi-Jun Mo [14], in which the parameters of a PEMFC model are determined and optimized by means of a hybrid genetic algorithm. Shan-Hai Ge and Bao-Lian Yi have proposed a model [15] that is both steady state and two-dimensional. This model studies the impact of factors such as flow mode (co-flow and counter-flow), operation conditions, and membrane thickness on the performance of PEMFC by analyzing aspects such as water transport, ohmic resistance, water and current density distribution. Another PEMFC performance model, this time based on empirical equations, is proposed by Kim et al [16]. Water flooding is also investigated: A research team from the University of Waterloo, led by J.J. Baschuk, developed a model [17] that takes into account the impact of varying levels of water flooding in the cathode catalyst layer. Another study about water flooding has been published by S. Shimpalee [18]. A work conducted by the University of Victoria [19] focused on exploring the structure and performance optimization of the cathode catalyst platinum and catalyst layer in a proton exchange membrane fuel cell. A recent review of the advancements in transport and diffusion modeling for PEM fuel cells is suggested in [20]. The literature includes various types of models, ranging from 0D to 3D models.

A multi-dimensional model is often necessary to gain an understanding of the detailed behavior of individual components, such as fuel cells, and to aid in designing for improved performance. Xing and Cai [21] developed a 2D model to examine how the relative humidity, stoichiometric flow ratio, channel length, and their interactions affect the performance of a PEM fuel cell. Meanwhile, Fuller and Newman [22] established a two-dimensional mass transport model for a membrane electrode assembly to assess the utilization of water, thermal energy, and reactants in fuel cells. In addition, D. Singh et al [23] proposed a two-dimensional model to simulate transport phenomena in a PEMFC. The model accounts for the diffusion of humidified fuel and oxidant gases through porous electrodes, as well as the convective and electro-osmotic transport of liquid water in the electrodes and the membrane. In order to solve the system of differential equations, Singh et al used a finite volume approach, and the model is validated using available experimental data. Finally, in reference [24], a 2D model was used to compute the performance of the cell, including its voltage-current density relationship, ohmic resistance, water distribution within the membrane, current distribution, and temperature changes along the gas channels. About 3D studies, Dumercy [25] developed a thermal model for two PEMFCs with power outputs of 150 and 500 W using a node network model, while S. Dutta et al [26] presented a 3D numerical model that forecasts the mass flow between the cathode and anode channels. However, when modeling an entire energy system, using a multi-dimensional approach can be demanding. Therefore, it's essential to have realistic modeling approaches that aren't excessively computationally intensive, making it feasible to develop whole-system models using commonly available computing resources.

As previously underlined, water and thermal management are critical factors for a proper design of a PEM fuel cell. An interesting paper [27] in which water management and control are studied, is made by Liyan Zhang et al. In the study a comprehensive model is built and based on this, a predictive control mechanism is proposed by utilizing Recurrent Neural Network (RNN) optimization. The MATLAB and SIMULINK environment is used for both the model and predictive controller. In the literature there are many studies about the thermal behavior of PEMFC systems. In general, the main cooling methods used are air and liquid cooling. K.P. Adzakpa et al. [28] have developed a 3D dynamic thermal finite difference model for a single fuel cell to analyze the temperature distribution in a fuel cell cooled from bottom to top using air. The model considers the thermal energy bal-

ance and accounts for the inlet gas humidity. The results indicate that the non-uniformity of temperature within the stack is quite significant. These temperature differences lead to substantial voltage disparities between the cells, resulting in reduced total electrical power output of the stack. Another study that shows the limits of the air cooling for PEM stacks is proposed by K. Ondrejička et al. [29]. Regarding liquid cooling techniques a detailed survey is made by Zhao X. et al [12]. Also Tiss [30] proposed a dynamic model for the thermal system of a PEMFC based on heat and mass transfer theory, which demonstrated the significance of fuel cell temperature in regulating its output voltage and gas flow. E. Hosseinzadeh et al [31] developed a general zero-dimensional PEMFC system model to investigate the effects of inlet and outlet temperatures and temperature gradient on system performance, revealing the importance of inlet air humidification. These models were designed to study the impact of thermal management on PEMFC system performance, but were not appropriate for controlling heat in a fuel cell system. A general review of PEM fuel system control is made by W.R.W. Daud [32]. In their work, Ahn et al. [33] put forward a novel approach to temperature control, utilizing a thermal circuit and employing classic proportional and integral (PI) controllers as well as state feedback control in the design. Meanwhile, X. Zhao et al. [12] established a water-cooled system model for thermal management control, based on electrochemical reactions and thermodynamics, and validated the model with an experimental system. Comparison of the model results and experimental data under various operating conditions demonstrated good agreement, indicating the model's accuracy in predicting the system behavior with the same control parameters. In some PEM systems, especially in light mobility application, the hydrogen source is obtained from a metal hydride tank. A general overview of requirements, materials and modelling approaches is presented by Pasini et al. [8]. Another study which evaluates the acceptability envelope for metal hydrides and their achievement of DOE technical standards is presented by Savannah River National Laboratory [34]. The modelling of metal hydrides is not trivial. It includes processes like temperature dependent chemical kinetic, thermodynamics, mass momentum and energy conservation. Parametric studies and simulations with experimental analysis are presented by Busqué et al. [35] and by Cho J. et al. [36]. Since the aim of the project is to build a comprehensive model which includes a metal hydride tank in the system, it is necessary to analyze the literature about coupling of fuel cell and the storage. A mathematical model was introduced in the paper [37]

by A. Tetuko et al. to examine a combined system of a PEM fuel cell and metal hydrogen storage. The system is interconnected by heat pipes, and the authors believe that the thermal coupling arrangement holds great potential. This is because as the PEMFC generates power, it also produces heat that can aid in accelerating the hydrogen release rate from the MH storage. D. Chabane et al. [9] also conducted a study on this type of coupling, where they utilized the heat generated by a PEMFC to warm a FeTi metal hydride. They performed simulations of the system using MATLAB/Simulink software and demonstrated that the proposed controller successfully accomplished two primary objectives: ensuring the consistent operation of both the PEMFC stack and MHT by maintaining their temperature and pressure levels. In their study, K. Malleswararao et al. [38] explored the thermodynamic compatibility criteria for selecting metal hydride pairs for use in thermal energy storage systems based on coupled metal hydrides. The researchers analyzed the performance of a coupled system using Mg2Ni for energy storage and LaNi5 for hydrogen storage. To simulate the system, a 3-D model was created and examined at charging and discharging temperatures of 300 °C and 230 °C, respectively, using COMSOL.

In the literature there are not many models based on Matlab ,Simulink or Simscape. An example is proposed by C. Mahjoubi et al. [39] in which a Simscape model is used to reproduce the stack dynamic behavior at different operating conditions and to simulate the temperature regulation and the air stoichiometric. Then, an experimental study is carried out by a 2 kW open cathode fuel cell system to validate the developed model and to evaluate the control strategy performance. Another Simscape model of a dynamic PEMFC thermal system is proposed by T. Kwan et al [40]. This paper proposes a thermal management system for a 500W fuel cell who exploits the characteristics of the thermoelectric device to achieve both temperature control and the possibility for energy harvesting when active control is not required. An experimental validation is made involving electric heaters to emulate the fuel cell's body heat. Other model based on Simulink are proposed by Politecnico di Milano [41] and M. Azri. et al [42].

Chapter 3

Simscape Model

Simscape allows you to quickly create models of physical systems in the Simulink environment. The Physical Network approach, which it employs, differs from the traditional Simulink modeling method, where each block symbolizes a basic mathematical operation, resulting in a diagram equivalent to the mathematical representation of the system being designed. Instead, Simscape represents each system as a set of functional elements that interact through exchanging energy via ports. This approach is well-suited for simulating systems with actual physical components. These connection ports are non-directional, resembling the connection of actual components, such as pumps and valves. Therefore, Simscape diagrams mimic the layout of the physical system, requiring no specification of flow directions or information flow during block connection. Once the simulation is initiated, the software solves a system of equations. Simscape is particularly well-suited for complex systems with multiple domains connected, such as thermal, liquid, and electrical domains. The choice of Simscape derives precisely from its capability to model more complex systems and their control, and also for the presence of a basic fuel cell model which exploits the foundation libraries. It is from this base model that the simulation of the system is built. It is also possible to create custom component models using a "MATLAB-based Simscape language", which enables text-based authoring of physical modeling components, domains, and libraries.

3.1 Membrane Electrode Assembly

The input for the model is the electrical load that the stack has to cover in terms of power. The electical power generated by the stack is:

$$Power_{elec} = (NViA)_{cell} \tag{3.1}$$

Where N_{cell} is the number of cells in the stack, i_{cell} is the current density of the cell, A_{cell} is the area of the cell and V_{cell} is the voltage of the single cell.

The voltage cell is equivalent to the Open Voltage Circuit (OCV) less the three over-voltages:

$$V_{cell} = V_{Nernst} - V_{Act} - V_{Ohm} - V_{cDiff} \tag{3.2}$$

The heat produced is equal to the power dissipated by the stack, so it is the difference between the net power generated and the electrical power:

$$P_{Diss} = Q = P_{Net} - P_{Elec} \tag{3.3}$$

The gas consumption and the water production per unit of time

$$H_{2,flow} = N_{cell} M_{H_2} A_{cell} \frac{i_{cell}}{2F} \tag{3.4}$$

$$O_{2,flow} = N_{cell} M_{O_2} A_{cell} \frac{i_{cell}}{4F} \tag{3.5}$$

$$H_2O_{flow} = N_{cell} M_{H_2O} A_{cell} \frac{i_{cell}}{2F} \tag{3.6}$$

Where F is the Faraday constant, equal to the electric charge per mole of elementary charges, and M is the molar mass.

The Nernst open circuit voltage is related to the operating temperature and the oxygen partial pressure in the cathode and the hydrogen partial pressure in the anode:

$$V_{Nernst} = \frac{RT_{Stack}}{2F} \ln\left(\frac{a_{H_2,a} a_{O_2,c}^{0.5}}{a_{H_2O,c}}\right) - \frac{G_{H_2O}}{2F} \tag{3.7}$$

G_{H2O} is the water Gibbs free energy of reaction, which is dependent on temperature and pressure of the stack. T_{Stack} is the stack temperature, R is the ideal gas constant. The letter a stands for the activity function, which is

in chemical thermodynamics a measure of the "effective concentration" of a species in a mixture. In general the subscript "a" stands for anode and "c" stands for cathode. The activity functions are function of the pressure and molar fraction. The anode and cathode pressures are:

$$p_c = \frac{p_{c_{in}} + p_{c,out}}{2} \tag{3.8}$$

$$p_a = \frac{p_{a_{in}} + p_{a,out}}{2} \tag{3.9}$$

The molar fractions at the anode and the cathode are:

$$y_{O_2,c} = \frac{y_{O_2,c,in} + y_{O_2,c,out}}{2} \tag{3.10}$$

$$y_{H_2,a} = \frac{y_{H_2,a,in} + y_{H_2,a,out}}{2} \tag{3.11}$$

$$y_{H_2O,c} = \frac{y_{H_2O,c,in} + y_{H_2O,c,out}}{2} \tag{3.12}$$

Activity functions:

$$a_{H_2,a} = \frac{y_{H_2,a} + P_a}{P_{std}} \tag{3.13}$$

$$a_{O_2,c} = \frac{y_{O_2,c} + P_c}{P_{std}} \tag{3.14}$$

$$a_{H_2O,c} = \frac{y_{H_2O,c} + P_{w,satur}}{P_{std}} \tag{3.15}$$

The activation polarization voltage is:

$$V_{Act} = \frac{RT}{2\alpha F} \ln \frac{i_{cell}}{i_o} \tag{3.16}$$

Where α is the charge transfer coefficient, which stands for the fraction of the interfacial potential at an electrode-electrolyte interface that helps in lowering the free energy barrier for the electrochemical reaction. The value i_o is the "Exchanged current", it is the basic current that exists always in the elctrode (both for open and closed circuit) due to continuos exchange of charges in the equilibrium of the reactions which occurs on the surface of catalyst grains.

The Ohmic Over-Voltage is:

$$V_{Ohm} = \frac{t_{memb}}{\sigma} i_{cell} \tag{3.17}$$

Where t_{memb} is the membrane thickness and σ is the membrane conductivity. The membrane conductivity depends on the water content of the membrane. The water content of the membrane is computed as a function of the water activity, assumed to be equal to the relative humidity ($R_{H,a,c}$). It is assumed that gas cannot permeate across the membrane [26].

For $R_H < 0$

$$\lambda = 17.81a + 0.043 \tag{3.18}$$

For $0 < R_H < 1$

$$\lambda = 17.81a + 0.043 - 39.85a^2 + 36a^3 \tag{3.19}$$

For $R_H > 1$

$$\lambda = 14.003 + 1.4(a - 1) \tag{3.20}$$

$$\lambda_{membrane} = \frac{\lambda_a + \lambda_c}{2} \tag{3.21}$$

For $\lambda_{membrane} > 1$

$$\sigma_{30} = 0.005139\lambda_{membrane} - 0.00326 \tag{3.22}$$

Else

$$\sigma_{30} = 0.005139 - 0.00326 \tag{3.23}$$

Finally the membrane conductivity:

$$\sigma = \sigma_{30} e^{\left(1268 * \left(\frac{1}{303.15} - \frac{1}{T_{Stack}}\right)\right)}; \tag{3.24}$$

Water diffusion coefficient across membrane is:

$$D_{H2O,memb} = 0.125 e^{2416\left(\frac{1}{303.15} - \frac{1}{T_{Stack}}\right)} \tag{3.25}$$

The water concentrations at anode and cathode catalyst layers:

$$Conc_{H2O,acl} = \frac{\rho_{membrane}}{M_{membrane}} \lambda_{acl} \tag{3.26}$$

$$Conc_{H2O,ccl} = \frac{\rho_{membrane}}{M_{membrane}} \lambda_{ccl} \tag{3.27}$$

Where $\rho_{membrane}$ is the density of the dry membrane and $M_{membrane}$ is the equivalent weight of the dry membrane. The Molar flux of water across membrane due to diffusion is:

$$\dot{n}_{H2O,diff} = D_{H2O,memb} \frac{(Conc_{H2O,acl} - Conc_{H2O,ccl})}{t_{memb}} \tag{3.28}$$

The molar flux of water across membrane due to hydraulic pressure difference based on Darcy's law:

For $p_A > p_C$

$$\dot{n}_{H2O,hydr} = (p_A - p_C) K_{darcy} p_a \frac{y_{H_2O,a}}{RT_{stack}\mu_{H2O} t_{memb}} \tag{3.29}$$

Else

$$\dot{n}_{H2O,hydr} = (p_A - p_C) K_{darcy} p_c \frac{y_{H_2O,c}}{RT_{stack}\mu_{H2O} t_{memb}} \tag{3.30}$$

K_{darcy} is the membrane permeability to water. The Water electro-osmotic drag coefficient is:

For $\lambda_a >= 0$

$$nd_{H_2O,membrane} = 0.0029\lambda_a^2 + 0.05\lambda_a \tag{3.31}$$

else

$$nd_{H_2O,membrane} = 0.05\lambda_a \tag{3.32}$$

The molar flux of water across membrane due to electro-osmotic drag:

$$\dot{n}_{H2O,drag} = nd_{H_2O,membrane} \frac{i_{cell}}{F} \tag{3.33}$$

The net water transport from cathode to anode is the sum of the flux of water across the membrane due to diffusion, electro-osmotic drag and hydraulic pressure difference based on Darcy's law:

$$H_2O_{trans} = (\dot{n}_{H2O,diff} + \dot{n}_{H2O,drag} + \dot{n}_{H2O,hydr}) N_{cell} M_{H_2O} A_{cell} \tag{3.34}$$

Energy generation due to reaction at standard temperature:

$$power_{rxn} = LHV_{H_2} \frac{H_{2,consumed}}{M_{H_2}} \tag{3.35}$$

Where LHV is low heating value of hydrogen. While the energy gain in membrane due to bringing reactants and products to standard temperature:

$$\begin{aligned} P_{\Delta std} = \dot{m}_{H_2}(h(T_{stack}) - h_{H_2,std}) \\ + \dot{m}_{O_2}(h_{O_2}(T_{stack}) - h_{O_2,std}) \\ + \dot{m}_{H_2O}(h_{H_2O}(T_{stack}) - h_{H_2O,std}) \end{aligned} \tag{3.36}$$

Energy gain in membrane due to water transport

$$P_{trans} = H_2O_{trans}(h_{w,S,a} - h_{w,vap,S,a}) - H_2O_{trans}(h_{w,S,c} - h_{w,vap,S,c}) \tag{3.37}$$

Where $h_{w,S}$ is the water vapour specific enthalpy and $h_{w,vap,S}$ is the water specific enthalpy of vaporization. Finally the Net energy gain in stack:

$$P_{net} = P_{rxn} + P_{\Delta std} + P_{trans} \tag{3.38}$$

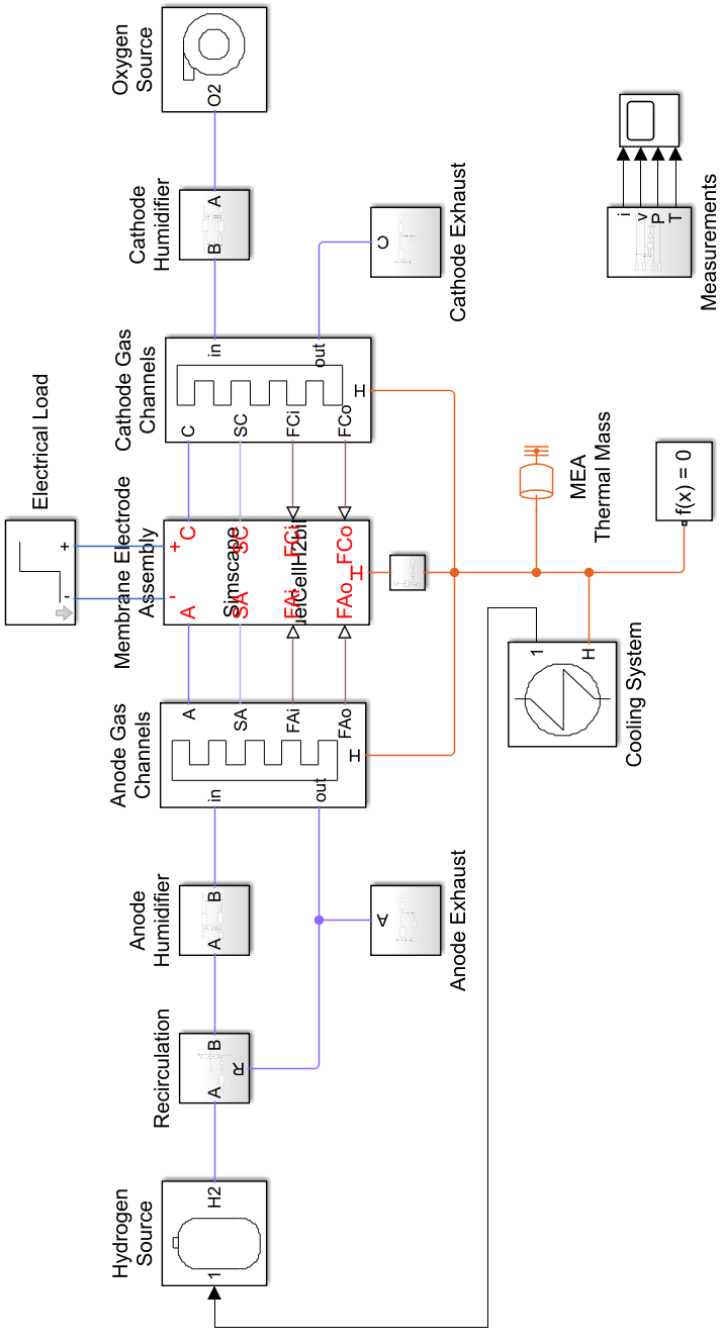

Figure 3.1: Simcape model including MEA, cooling system, anode and cathode channels

3.2 Anode and Cathode Channels

The anode and cathode channels, both inside the stack and outside at the source/exhaust pipes are modelled with Simscape using the component "Pipe". This component models the dynamic flow of the fluid taking care of the viscous losses and the convective heat transfer with the wall [43] [44] [45]. Here are the assumptions and limitations of the model:

- The pipe wall is perfectly rigid.
- The flow is fully developed.
- The effect of gravity is negligible.
- Fluid inertia is negligible. (Moist air domain only)
- No supersonic flow. (Moist air domain only)

The net flow rates into the volume inside the pipes are:

$$\dot{m}_{\text{net}} = \dot{m}_A + \dot{m}_B - \dot{m}_{\text{cond}} \tag{3.39}$$

$$\Phi_{\text{net}} = \Phi_A + \Phi_B + Q_{wall} - \Phi_{\text{cond}} \tag{3.40}$$

$$\dot{m}_{w,\text{ net}} = \dot{m}_{wA} + \dot{m}_{wB} - \dot{m}_{\text{cond}} \tag{3.41}$$

$$\dot{m}_{g,net} = \dot{m}_{gA} + \dot{m}_{gB} \tag{3.42}$$

Where the subscript "A" stand for inlet, "B" stands for outlet, "I" for internal node. "a" is dry air, "g" is trace gas and "w" stands for water vapor. The $\dot{m}_{cond}$ is the rate of condensation, equal to:

$$\dot{m}_{\text{cond}} = \begin{cases} 0, & \text{if } x_{w,I} \leq x_{ws,I} \\ \frac{x_w - x_{ws,I}}{\tau_{\text{condense}}} \rho_I V, & \text{if } x_{w,I} > x_{ws,I} \end{cases} \tag{3.43}$$

τ_{cond} is the condensation time constant parameter. x_w is the specific humidity of the fluid in the tube, while x_{ws} is the specific humidity at saturation:

$$x_{ws,I} = \frac{R_I}{R_w} \frac{p_{ws,I}}{p_I} \tag{3.44}$$

$p_{ws,I}$ is the water vapor pressure at the fluid temperature T_I, while R_I is the mixture specific gas constant, equal to:

$$R_I = x_{w,I}R_w + x_{a,I}R_a + x_{g,I}R_g \tag{3.45}$$

$$x_{g,I} + x_{a,I} + x_{w,I} = 1 \tag{3.46}$$

Φ_{cond} is the rate of energy loss due to the condensation of the water:

$$\Phi_{cond} = \dot{m}_{cond}(h_{w,I} - \Delta h_{vap,I}) \tag{3.47}$$

Where $\Delta h_{vap,I}$ is the specific enthalpy of vaporization. The energy exchanged at the port inlet A and outlet B half pipes is:

$$\Phi_A = h_A - h_I = \left(\frac{R_I \dot{m}_A}{S}\right)^2 \left[\left(\frac{T_I}{p_I}\right)^2 - \left(\frac{T_A}{p_A}\right)^2\right] \tag{3.48}$$

$$\Phi_B = h_B - h_I = \left(\frac{R_I \dot{m}_B}{S}\right)^2 \left[\left(\frac{T_I}{p_I}\right)^2 - \left(\frac{T_B}{p_B}\right)^2\right] \tag{3.49}$$

h is the specific enthalpy. The heat exchanged with the wall is the sum of the conduction and convection contributions:

$$Q_{wall} = Q_{cond} + Q_{conv} \tag{3.50}$$

The conduction heat is evaluated by using the classic Fourier relation:

$$Q_{cond} = k_I \frac{A_S}{D_h}(T_{wall} - T_I) \tag{3.51}$$

k is the thermal conductivity, A_S is the heat schange surface and D_h is the hydraulic diameter.

For the convective heat exchanged, the effectiveness-NTU method is used. The Darcy friction factor in the turbulent regime is, according to the Haaland correlation:

$$f = \frac{1}{\left[-1.8 \log_{10}\left(\frac{6.9}{\mathrm{Re}} + \left(\frac{1}{3.7}\frac{r}{D_h}\right)^{1.11}\right)\right]^2} \tag{3.52}$$

Where r is the surface roughness. The Reynolds number is:

$$Re = \frac{\dot{m} D_h}{A\mu} \tag{3.53}$$

The turbulent pipe flow Nusselt number using the Gnielinski correlation is:

$$Nu_{\text{tur}} = \frac{\frac{f}{8}\left(\text{Re} - 1000\right)\text{Pr}}{1 + 12.7\sqrt{\frac{f}{8}}\left(\text{Pr}^{2/3} - 1\right)} \tag{3.54}$$

The Nusselt number of the fluid is obtained blending, according to the flow regime (Reynolds Number), between the the laminar value and the turbulent one. The following function simply makes this blending assuring the continuity and differentiability of Nu in the interval:

$$\begin{aligned} Nu = & \left(1 - 3\frac{Re - Re_{lam}}{Re_{tur} - Re_{lam}}^2 + 2\frac{Re - Re_{lam}}{Re_{tur} - Re_{lam}}^3\right) Nu_{lam} \\ & + \left(3\frac{Re - Re_{lam}}{Re_{tur} - Re_{lam}}^2 - 2\frac{Re - Re_{lam}}{Re_{tur} - Re_{lam}}^3\right) Nu_{tur} \end{aligned} \tag{3.55}$$

The number of transfer unit is:

$$NTU = \frac{NuA_S}{Prk_I A} \tag{3.56}$$

We can consider the pipe as a so called "single-stream heat exchanger" in which one of the heat exchanger fluids has no mass flow (like the solid wall of the pipe) [46]. For this case the effectiveness is given by:

$$\epsilon = 1 - e^{-NTU} \tag{3.57}$$

Finally the convection heat is:

$$Q_{conv} = \epsilon \dot{m} c_p (T_{wall} - T_I) \tag{3.58}$$

The pressure losses are evaluated blending the losses between the laminar and turbulent regime. The laminar viscous loss is:

$$\Delta p_{lam} = \frac{\dot{m}\mu s_f L}{2\rho D_h^2 A} \tag{3.59}$$

Where s_f is the laminar friction constant for Darcy friction factor. The turbulent friction loss is:

$$\Delta p_{tur} = \frac{\dot{m}\mu f L}{2\rho D_h^2 A} \tag{3.60}$$

Where f is the Darcy friction factor expressed in the equation 3.52. Finally the friction loss is blended between the laminar and turbulent regime:

$$\begin{aligned}\Delta p = & \left(1 - 3\frac{Re - Re_{lam}}{Re_{tur} - Re_{lam}}^2 + 2\frac{Re - Re_{lam}}{Re_{tur} - Re_{lam}}^3\right)\Delta p_{lam} \\ & + \left(3\frac{Re - Re_{lam}}{Re_{tur} - Re_{lam}}^2 - 2\frac{Re - Re_{lam}}{Re_{tur} - Re_{lam}}^3\right)\Delta p_{tur}\end{aligned} \tag{3.61}$$

The equations related to moist air pipe control volume are:

1. Water mass vapor conservation:

$$\frac{dx_{wI}}{dt}\rho_I V + x_{wI}\dot{m}_{net} = \dot{m}_{w,net} \tag{3.62}$$

2. Trace gas mass conservation:

$$\frac{dx_{gI}}{dt}\rho_I V + x_{gI}\dot{m}_{net} = \dot{m}_{g,net} \tag{3.63}$$

3. Mixture mass conservation::

$$\begin{aligned}\left(\frac{1}{p_I}\frac{dp_I}{dt} - \frac{1}{T_I}\frac{dT_I}{dt}\right)\rho_I V + \frac{R_a - R_w}{R_I}\left(\dot{m}_{w,net} - x_w\dot{m}_{net}\right) \\ + \frac{R_a - R_g}{R_I}\left(\dot{m}_{g,net} - x_g\dot{m}_{net}\right) = \dot{m}_{net}\end{aligned} \tag{3.64}$$

4. Energy conservation:

$$\begin{aligned}\rho_I c_{vI} V\frac{dT_I}{dt} + \left(u_{wI} - u_{aI}\right)\left(\dot{m}_{w,net} - x_w\dot{m}_{net}\right) \\ + \left(u_{gI} - u_{aI}\right)\left(\dot{m}_{g,net} - x_g\dot{m}_{net}\right) + u_I\dot{m}_{net} = \Phi_{net}\end{aligned} \tag{3.65}$$

Where u is the specific internal energy.

For the thermal liquid domain the system of equation is:

1. The mass conservation equation under the hypothesis of no dynamic comressibility:
$$\dot{m}_{\mathrm{A}} + \dot{m}_{\mathrm{B}} = 0 \tag{3.66}$$

2. Energy conservation equation:
$$V\frac{d(\rho u)}{dt} = \Phi_A + \Phi_B + Q_{wall} \tag{3.67}$$

3. Momentum equation for the two half-pipes:
$$p_A - p_I = \Delta P_A \tag{3.68}$$
$$p_B - p_I = \Delta P_B \tag{3.69}$$

Friction losses and heat exchanged are evaluated with the same equations of the moist air domain. All the fluid's properties are tabled.

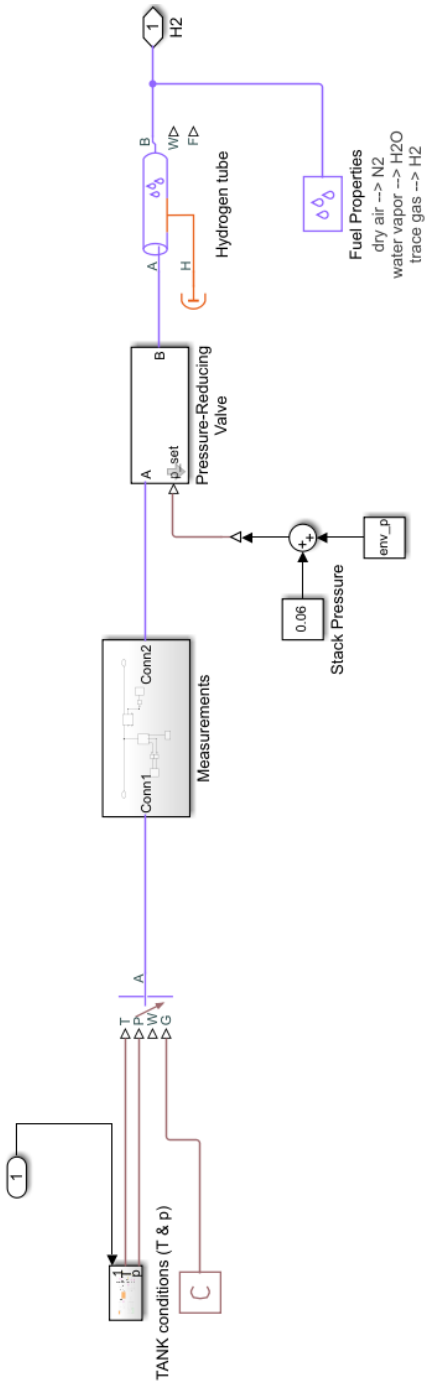

Figure 3.2: Hydrogen source with pressure-reducing valve

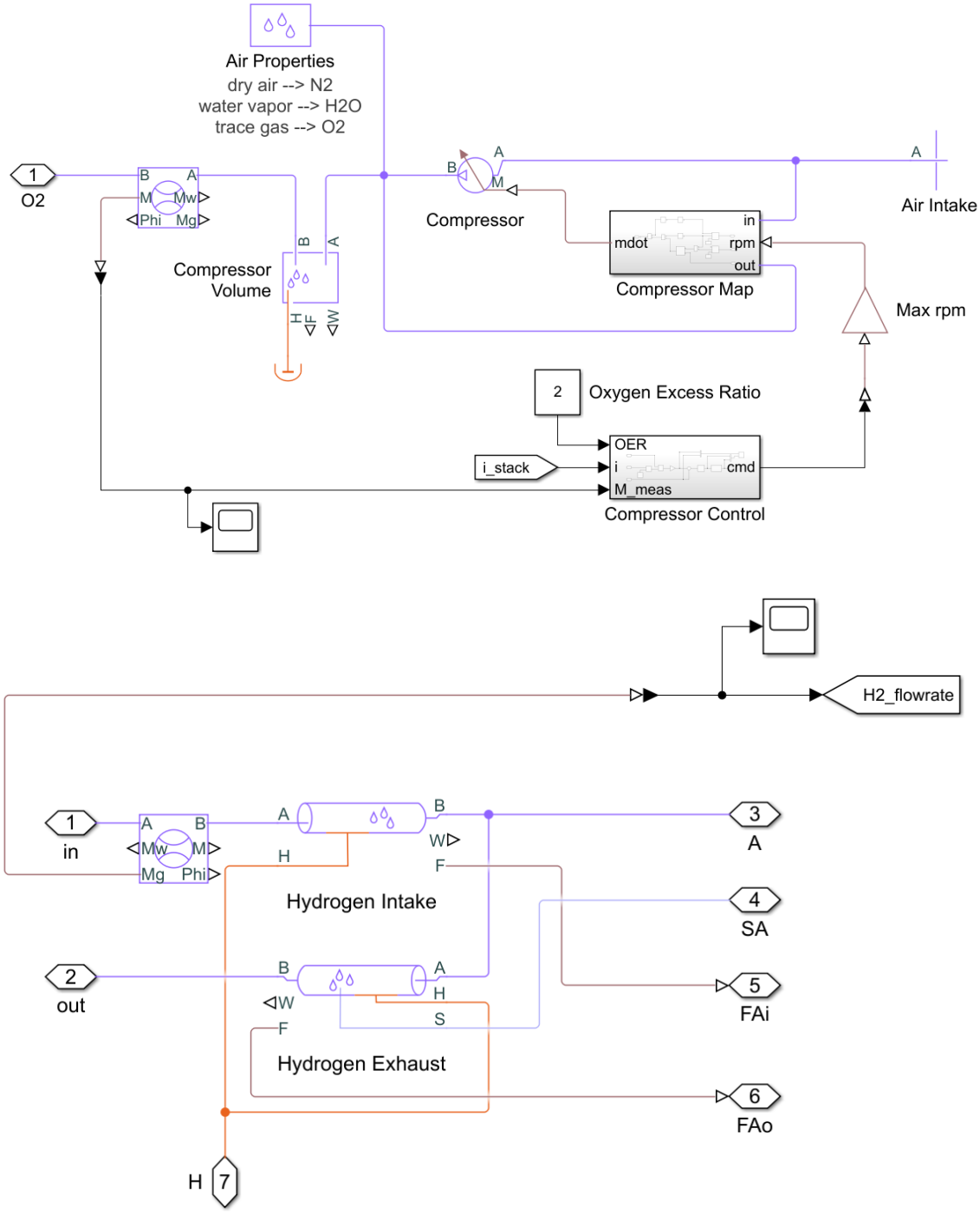

Figure 3.3: Air source with blower (above). Anode channels in the stack(below)

3.3 Cooling System

As the fuel cell over-heating has to be avoided, a cooling system strategy, control and model is necessary. The heat produced by the stack is evaluated in the Membrane Electrode Assembly model paragraph [3.1], and the increasing temperature stack's mass is modelled in Simscape by the thermal mass component:

$$Q_{net} = m_{stack} c_{p,stack} \frac{dT_{stack}}{dt} \tag{3.70}$$

Where m_{stack} is the stack weight, $c_{p,stack}$ is its specific heat capacity and Q_{net} is the net heat equal to the heat produced by the stack less the heat dissipated by the cooling system. The heat exchanged by the stack to the coolant water is modelled with the pipe component in the thermal liquid domain (see [3.2]). Input parameters are:

$$Pipe_{length} = n_{coolant} \sqrt{A_{stack}} \tag{3.71}$$

Where A_{stack} is the area of the cell and $n_{coolant}$ is the number of coolant passes in the cell. The cross-sectional area is:

$$A_{cross} = w_{coolant}^2 n_{coolant,layer} \tag{3.72}$$

$w_{coolant}$ is the coolant channels width, $n_{coolant,layer}$ is the number of coolant layers. Hydraulic diameter:

$$D_h = w_{coolant} \tag{3.73}$$

No convective heat transfer between the stack and the environment is considered. The heat losses at the cooling circuit are accounted in a thermal liquid pipe with a thermal mass which exchanges heat to the environment by natural convection. The thermal mass is the radiator mass, the heat transfer surface is the radiator surface and the heat transfer coefficient is the natural convection coefficient, usually between 3 and 10 $\frac{W}{Km^2}$.

The air to water heat-exchanger is modelled with a component present in the Simscape library called "Heat exchanger MA-TL". The method used for the the heat rate exchange evaluation is the $\epsilon - NTU$. For a cross-flow arrangement with mixed air and unmixed water, the effectiveness is:

$$\epsilon = 1 - e^{\frac{1}{C_R}\left(1 - e^{-C_R NTU}\right)} \tag{3.74}$$

Where C_R is the ratio between heat capacity rates:

$$C_{min} = \dot{m}_{air} c_{p,air} \tag{3.75}$$

$$C_{max} = \dot{m}_{coolant} c_{p,water} \tag{3.76}$$

The number of transfer unit NTU is:

$$NTU = \frac{1}{C_{min} R} \tag{3.77}$$

And finally the heat transfer:

$$Q_{hx} = \epsilon C_{min} (T_{coolant,in} - T_{amb}) \tag{3.78}$$

All the input parameters are listed in table 3.5.2. In the figure 3.4 is represented the Simscape layout of the cooling system.

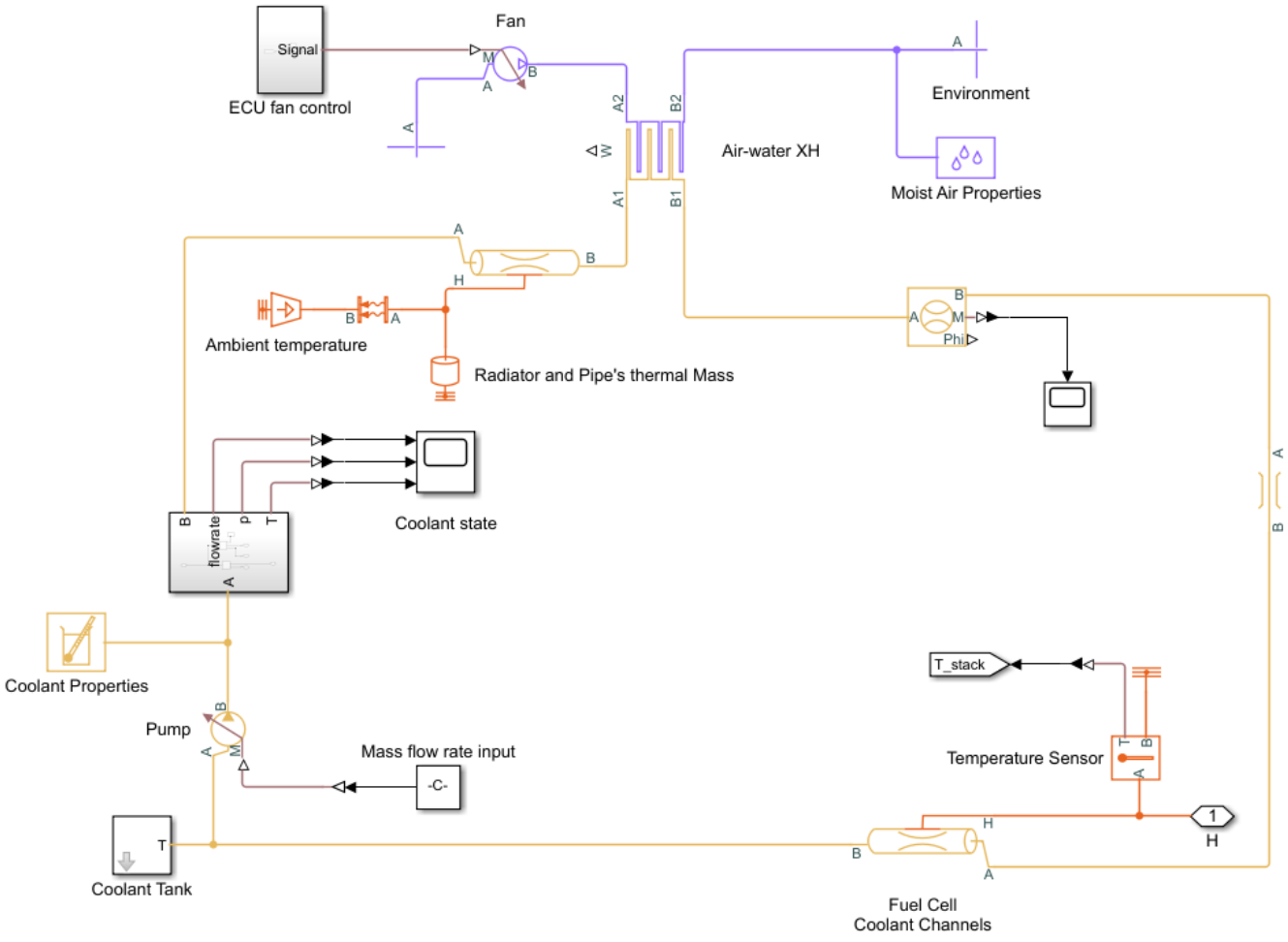

Figure 3.4: Cooling system with coolant channels(modeled as pipe), pump, radiator and tubes

3.3.1 Metal Hydride Tank

The metal hydride tank consists in a shell in which the thermal fluid passes through a bank of tubes containing the metal hydride powder. This tank can be seen like a baffled shell and tube heat exchanger" in which there is no stream inside the tubes as the metal powder is solid. The modelling of this system can be performed in the same way as the radiator or the pipe in the thermal liquid domain (effectiveness-NTU in one stream heat exchanger) [see paragraph 3.2], the problem is that the convective heat transfer coefficient of the thermal fluid flowing in the shell is not known, so in order to evaluate it, the so called "Bell-Delaware method" is used. This method employs empirical correction factors to calculate heat transfer for a flow perpendicular to a bank of tube, called ideal flow. However, in the baffle windows, the flow is partially parallel to the tubes. Moreover, due to leakage and bypass streams in the shell, only a portion of the shell-side fluid follows the primary flow path through the exchanger. Correction factors for heat transfer and pressure drop account for these deviations from ideal tube bank conditions.

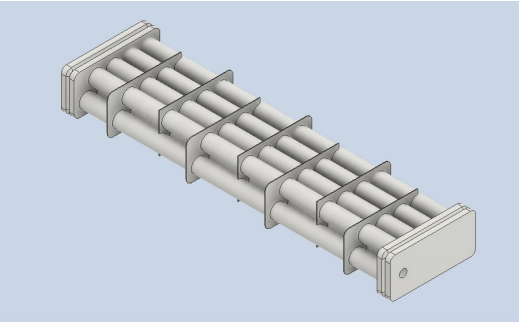

Figure 3.5: Hydride tank

G_s is the mass velocity in the shell equal to:

$$G_s = \frac{\dot{m}}{A_s} \tag{3.79}$$

Where A_s is the cross-flow section of the ideal tube bank through which flows the thermal fluid:

$$A_s = b\left(\left(h_s - h_{otl} - \frac{d_o}{2}\right) + h_{otl}\frac{(p_t - d_o)}{pt}\right) \tag{3.80}$$

Where d_o is the outer diameter of the hydride tube. b is the baffle spacing, h_s is the height of the shell, h_{otl} is the height distance of the outer tubes in the bank and p_t is the transverse tube pitch. The Reynolds number is evaluated as follow:

$$Re = \frac{d_o G_s}{\mu} \tag{3.81}$$

In order to calculate the Colburn factor j, empirical coefficients are needed, these can be seen in the following table based on Reynolds number and layout angle of tubes:

height	Layout angle	Reynolds number	a_1	a_2	a_3	a_4
30°		$10^5 - 10^4$	0.321	-0.388	1.450	0.519
		$10^4 - 10^3$	0.321	-0.388		
		$10^3 - 10^2$	0.593	-0.477		
		$10^2 - 10$	1.360	-0.657	< 10	1.400
45°		$10^5 - 10^4$	0.370	-0.396	1.930	0.500
		$10^4 - 10^3$	0.370	-0.396		
		$10^3 - 10^2$	0.730	-0.500		
		$10^2 - 10$	0.498	-0.656		
		< 10	1.550	-0.667		
90°		$10^5 - 10^4$	0.370	-0.395	1.187	0.370
		$10^4 - 10^3$	0.107	-0.266		
		$10^3 - 10^2$	0.408	-0.460		
		$10^2 - 10$	0.900	-0.631		
		10	0.970	-0.667		

Finally the Colburn factor and the ideal heat transfer coefficient:

$$a = \frac{a_3}{1 + 0.14(Re)^{a_4}} \tag{3.82}$$

$$j = a_1 \left(\frac{1.33}{P_T/d_o} \right)^a (Re)^{a_2} \tag{3.83}$$

$$\mathrm{h_{id}} = \mathrm{jG_s c_p \, Pr^{-\frac{2}{3}}} \tag{3.84}$$

Where c_p is the heat capacity of the thermal fluid and Pr is the Prandtl number. The ideal heat transfer coefficient needs to be corrected by different correction factors:

$$h_o = h_{\text{ideal}} \ (J_C J_L J_B J_R) \tag{3.85}$$

The correction factor for the baffle window flow takes care of the portion of the flow in which the fluid is parallel to the tubes:

$$J_C = 0.55 + 0.72x_c \tag{3.86}$$

x_c is the fraction of tubes in cross-flow. The correction factor J_L of the shell-to-baffle leakage is:

$$J_L = 0.44(1 - r_s) + (1 - 0.44(1 - r_s))e^{-2.2r_l} \tag{3.87}$$

Where

$$\begin{aligned} r_s &= \frac{S_{sb}}{S_{sb} + S_{tb}} \\ r_l &= \frac{S_{sb} + S_{tb}}{S_m} \end{aligned} \tag{3.88}$$

S_{sb} is the shell-to-baffle leakage area and S_{tb} is the tube-to-baffle leakage area:

$$S_{sb} = d_{bs}(2w_s - 2b_c + h_s - 2d_{bs}) \tag{3.89}$$

$$S_{tb} = \frac{pi}{4}\left((do + d_{tb})^2 - d_o^2\right) n_{tubes}\left(1 - \frac{(1 - x_c)}{2}\right) \tag{3.90}$$

d_{bs} is the gap between the baffle and the shell, w_s is the width of the shell, b_c is the baffle cut and d_{tb} is the gap between the tube and the bundle. The correction factor J_B express the bundle-to-shell by-pass flow:

$$\begin{aligned} &J_B = \exp\left[-C_J\left(S_b/S_m\right)\left(1 - \sqrt[3]{2r_{ss}}\right)\right] && \text{for } r_{ss} < 0.5 \\ &J_B = 1.0 && \text{for } r_{ss} \geq 0.5 \end{aligned} \tag{3.91}$$

Where

$$\begin{aligned} &C_J = 1.35 && \text{for } Re \leq 100 \\ &C_J = 1.25 && \text{for } Re > 100 \end{aligned} \tag{3.92}$$

And

$$r_{ss} = \frac{N_{ss}}{N_c} \tag{3.93}$$

N_{ss} is the number of pairs of sealing strips and N_c is the number of effective tube rows in cross section. Finally the correction factor of the laminar flow J_R:

$$\begin{array}{ll} J_R = (10/N_{ct})^{0.18} & \text{for } Re \leq 20 \\ J_R = 1.0 & \text{for } Re \geq 100 \end{array} \tag{3.94}$$

N_{ct} is the total number of tube rows crossed:

$$N_{ct} = N_{rw} + N_c; \tag{3.95}$$

Where N_{rw} is the number of tubes crosssing the baffle window. The overall heat transfer coefficient U is:

$$\mathrm{U_0} = \frac{1}{\frac{1}{h_o} + \frac{\mathrm{d_o}\ln\left(\frac{\mathrm{d_o}}{\mathrm{d_i}}\right)}{2\mathrm{k_W}}} \tag{3.96}$$

Where k_w is the conductive heat transfer coefficient of the tube and d_i is the inner diameter. The number of heat transfer unit is:

$$NTU = \frac{UL_s n_{tubes} d_o}{\dot{m} c_p} \tag{3.97}$$

Where L_s is the shell length equal to the legnth of the tubes. The effectiveness ϵ is the one of the single stream heat exchanger [see 3.57]. Finally the convective heat exchanged by the thermal fluid to the MH is:

$$Q_{tank} = \epsilon c_p \dot{m} (T_{hyd} - T_I) \tag{3.98}$$

Where T_{hyd} is the temperature of the hydrides evaluated in 3.107 and T_I is the temperature of the tank node inside the Simscape network. A Simscape component which represent this kind of exchanger does not exist in the libraries, so a new component code is built by using the ssc code.

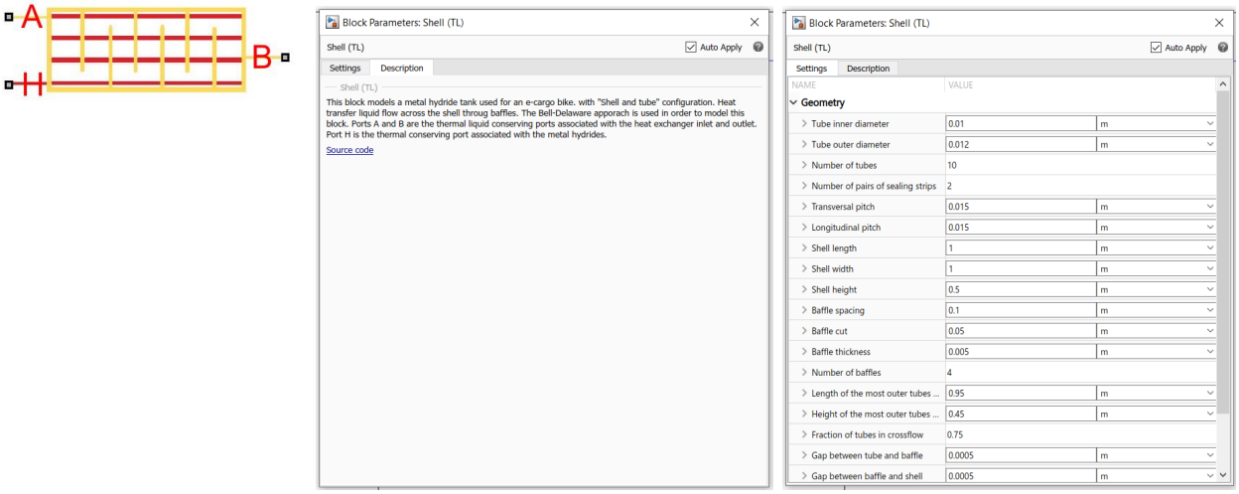

Figure 3.6: Hydride tank in simscape

3.4 Metal Hydride Tank

The metal hydride tank model proposed is based on the "H2 Vehicle Simulation Framework" made by DOE. This model is modified in order to fit better the e-cargo-bike system. The aim of the model is to simulate and control the dynamic processes of hydrogen discharge from a metal hydride tank during the operation of the stack.

The assumptions made in the model are the following:

1. Hydrogen is considered to be an ideal gas.
2. Powdery metal hydride is isotropic and homogeneous porous medium.
3. Local thermal equilibrium is assumed between the solid metal and the hydrogen gas. This means that the gas and metal local temperatures inside the vessel will be the same.
4. No radiative heat exchange inside the vessel.
5. Volumetric compression of the metal hydride during desorption is neglected.
6. Metal hydride properties such as porosity, permeabilityand thermal conductivity remain constant during the desorption process.

7. The thermal conductivity and the specific heat are assumed to remain constant during the storage/release process.

The input in the model is the H_2 flow rate consumed by the stack, obtained from the equation 3.4. The hydrogen flow rate which is desorbed from the metal hydride is the product of the metal hydride total mass m_{hyd} and the variation of hydrogen weight fraction per unit of time:

$$H_{2,flow,HG} = \frac{m_{hyd}\frac{dwf}{dt}}{0.002} \tag{3.99}$$

The pressure in the vessel is evaluated using the ideal gas equation as following:

$$p_{hyd} = \left(H_{2,0} + \int_{t_0}^{t} \frac{H_{2,flow,HG} - H_{2,flow}}{V_{free}}\, dt \right) RT_{hyd} \tag{3.100}$$

Where $H_{2,0}$ is the initial number of moles in the free volume, V_{free} is the free volume, R is the gas constant and T_{hyd} is the temperature of the MH/gas. The initial moles of hydrogen per unit volume is:

$$H_{2,0} = \frac{p_0}{RT_0} \tag{3.101}$$

Where P_0 and T_0 are respectively the initial pressure and initial temperature in the vessel. The reaction rate is evaluated as follow:

$$\begin{aligned} \frac{dwf}{dt} = &- \operatorname{sgn}\left(\frac{wf}{wf_{\text{full}}} - x_{\text{sat}} \right) wf_{\text{full}}\, Ae^{-E_a/RT_{hyd}} \\ &\left| \ln\left(\frac{p_{hyd}}{p_{\text{sat}}\,(T_{hyd})} \right) \right| \left| \frac{wf}{wf_{\text{full}}} - x_{\text{sat}} \right|^{\chi} \end{aligned} \tag{3.102}$$

Where χ is the order of forward reaction, wf is the weight fraction and wf_{full} is the maximum net weight fraction of hydrogen. p_{sat} is the equilibrium pressure evaluated as follow:

$$p_{sat} = e^{\frac{\frac{\Delta H_{P,eq}}{T_{hyd}} - \Delta S_{eq}}{R}} \tag{3.103}$$

The actual weight fraction is obtained by integrating over time the reaction rate:

$$wf = wf_0 + \int_{t_0}^{t} \frac{dwf}{dt}\, dt \tag{3.104}$$

The desorption of hydrogen is an exothermic reaction, and the produced heat rate per unit of mass is:

$$H_{reac,m} = \frac{\Delta H_{H_2}}{0.002} \frac{dwf}{dt} \tag{3.105}$$

Where ΔH_{H_2} is the heat of reaction per unit mole. The net heat taken by the metal hydride is:

$$Q_{net} = Q_{tank} - m_{hyd} H_{reac,m} \tag{3.106}$$

Where Q_{tank} is the heat exchanged by the tank inside the thermal system evaluated in 3.98. Finally, the temperature of the hydrogen is:

$$T_{hyd} = T_0 + \int_{t_0}^{t} \frac{Q_{net}}{c_{p,hyd}}\, dt \tag{3.107}$$

On figure 3.7 it its possible to see the flow-chart representing the model. Violet blocks are input, while yellow block are processes.

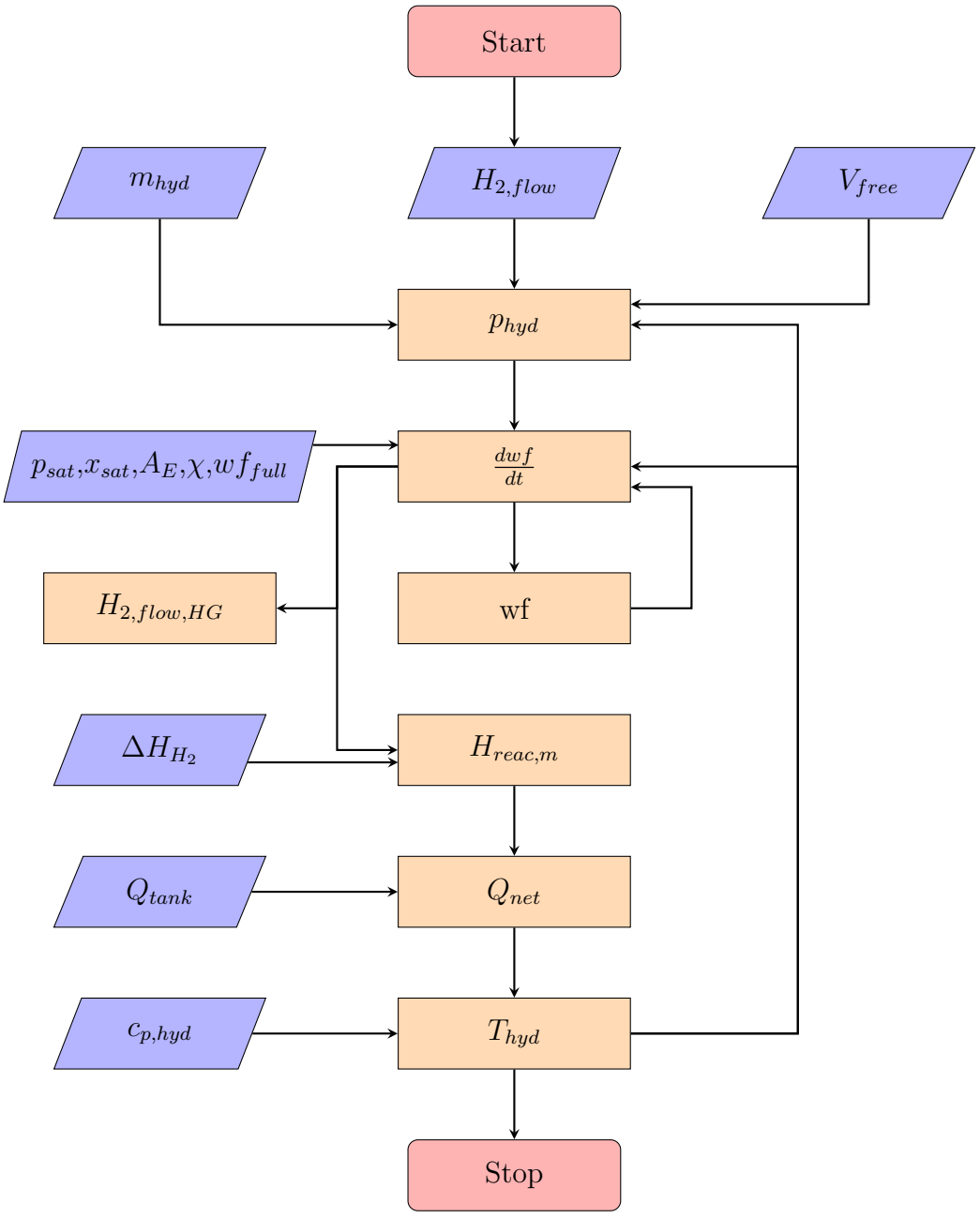

Figure 3.7: Flow chart of the Simulink model for the metal hydride tank

3.5 Parameters

Parameters are one of the most important factor for a model, especially when we are dealing with a component oriented software like Simscape. The system we want to model is composed by many object and components that require a lot of information in order to be well built: some of these information are obtained from data-sheets, some are taken from literature, some other are assumed.

3.5.1 Membrane Electrode Assembly

The number of cell in the stack, the membrane area and thickness are given by data-sheet. The gas diffusion layer is not given by the costructor, but in the literature it is found that the typical thickness for GDL is between 150 and 400 μm [47]. In the study conducted by Cindrella et al. [48] on a stack with similar characteristic of our system, the GDL thickness is $235\mu m$, so this is the assumed value for the stack. The channel width inside the bipolar plates is also not given, in the literature the channel width is in a range from 0.3 to 2 mm (parametric study of the channel width ranging from 0.3 to 1mm [49] and from 0.2 to 2 mm [50]). In general the most common width seen in literature is $1mm$, examples are in [51] and [52]. In the just cited studies the number of channels is given in a range between 12 and 36, also different configurations are possible (parallel, serpentine, etc.)

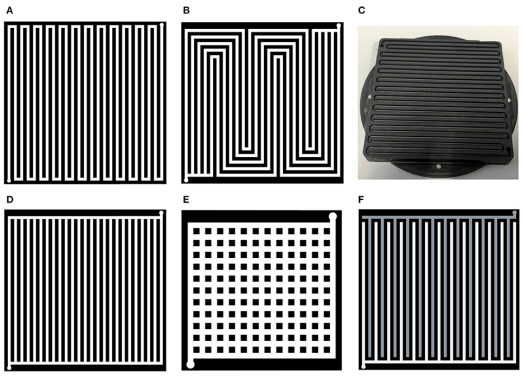

Figure 3.8: Bipolar plate channel configurations

As soon as the configuration of channels is serpentine (from the datasheet) one of the most common values for the number of channel is 20, this is the assumed value. About the cooling channels, E. Ashfare et al have proposed a parametric study [53] on cooling channels dimension, in this study is showed that increasing the channel width more than 3 mm does not improve the cooling performance, and the width of 1 mm is recommended. In the same paper it is said that the distance between two cooling channels should be lower

than 2 mm. Again, in the studies above cited, the most common value for coolant channel is 1mm. The number of coolant channels is assumed by length of the bipolar plate and the maximum distance allowed for the cooling channels. The electro-chemical parameters such as exchanged current density i_o, limiting current density i_L, charge transfer coefficient α, water diffusivity in GDL D_{gdl}, membrane's density ρ_{memb}, equivalent weight of the dry membrane mem_{MW}, overall membrane's density ρ_{mea}, overall specific heat of mea $c_{p,mea}$ are all well known and pretty constant through the literature.

Parameter	Value	Unit	Source
Number of cells	30	-	Data-sheet
Cell area	31.5	cm^2	Data-sheet
Membrane thickness	125	μm	Data-sheet
GDL thickness	235	μm	Literature
Channel width	0.1	cm	Literature
Channel number in the stack	20	-	Hypothesis
Coolant channel width	0.1	cm	Literature
Exchange current density	0.0001	$\frac{A}{cm^2}$	Literature
Limiting current density	1.4	$\frac{A}{cm^2}$	Literature
Charge transfer coefficient	0.5	-	Literature
Water vapour diffusivity in GDL	0.07	$\frac{cm^2}{s}$	Literature
Density of dry membrane	2000	$\frac{kg}{m^3}$	Assumption
Equivalent weight of dry membrane	1.1	$\frac{kg}{mol}$	Literature
Stack weight	2	kg	Data-sheet
Overall MEA c_p	1100	$\frac{J}{kgK}$	Literature
Anode tube diameter	0.007	m	Data-sheet
Cathode tube diameter	0.007	m	Data-sheet

3.5.2 Cooling System

Cooling system's parameter are mostly given by data-sheet of the system to be simulated. The coolant is water, the flow rate depends on the pressure losses in the circuit which are not well known, so it is measured experimentally. Other important parameters experimentally evaluated are heat transfer coefficient and surface area of radiator and mass flow rate of the air produced by the fans. [see paragraph 4.3]

Parameter	Value	Unit	Source
Coolant tube diameter	0.007	m	Data-sheet
Radiator length	0.167	m	Data-sheet
Radiator width	0.04	m	Data-sheet
Radiator height	0.08	m	Data-sheet
Radiator number of tubes	8	-	Data-sheet
Radiator tubes distance	0.0033	m	Data-sheet
Radiator η fin	0.7	-	Hypothesis
Radiator wall thickness	0.001	m	Hypothesis
Radiator weight	0.556	kg	Data-sheet
Radiator c_p	390	$\frac{J}{kgK}$	Data-sheet
Radiator fin spacing	0.0015	m	Measured
Radiator thermal resistance	$3.45x10^{-5}$	$\frac{K}{kW}$	Measured
Air flow rate	0.042	$\frac{kg}{s}$	Measured

3.5.3 Metal hydrides

Metal hydridse tank's parameter are taken, again, from data-sheet, literature or hypothesis. The parameters are design parameters (tank, material, refueling conditions) and kinetic parameters. Specification, value and source/references are all summed in the following table:

Parameter	Value	Unit	Source
Storage material content	0.11	kg	Data-sheet
Hydrogen weight fraction	0.01	–	Data-sheet
Metal density	8400	$\frac{kg}{m^3}$	Ref. [54], [55], [56]
Inert material density	2100	$\frac{kg}{m^3}$	Ref. [54]
Porosity	0.5	-	Ref. [55], [56]
Refueling temperature	390	$\frac{J}{kgK}$	Data-sheet
Refueling pressure	390	$\frac{J}{kgK}$	Data-sheet
Refueling pressure	390	$\frac{J}{kgK}$	Data-sheet
Hydride specific heat	390	$\frac{J}{kgK}$	Ref. [55], [56]
Activation energy of the forward reaction	21.170	$\frac{kJ}{mol}$	Ref. [56]
Activation energy of the backward reaction	16.420	$\frac{kJ}{mol}$	Ref. [56]
Reaction enthalpy	30.8	$\frac{kJ}{mol}$	Ref. [54], [55], [56]
Reaction entropy	0.108	$\frac{kJ}{molK}$	Ref. [54], [55], [56]
Forward rate constant	59.187	$\frac{1}{s}$	Ref. [56]
Backward rate constant	9.57	$\frac{1}{s}$	Ref. [56]
Order of the forward reaction	1	-	Hypothesis
Order of the backward reaction	1	-	Hypothesis

3.6 Results

A run of the model is performed by taking as input a step current with a jump from 0 A to 18 A and a ramp from 0A to 30A. In figure 3.9, as the current goes up, the voltage drops. It is also present the typical under-shoot that the voltage do as the current demand suddenly changes.The control of the fan seems to work properly, as the heat dissipation is enough to guarantee the avoidance of over-temperatures.

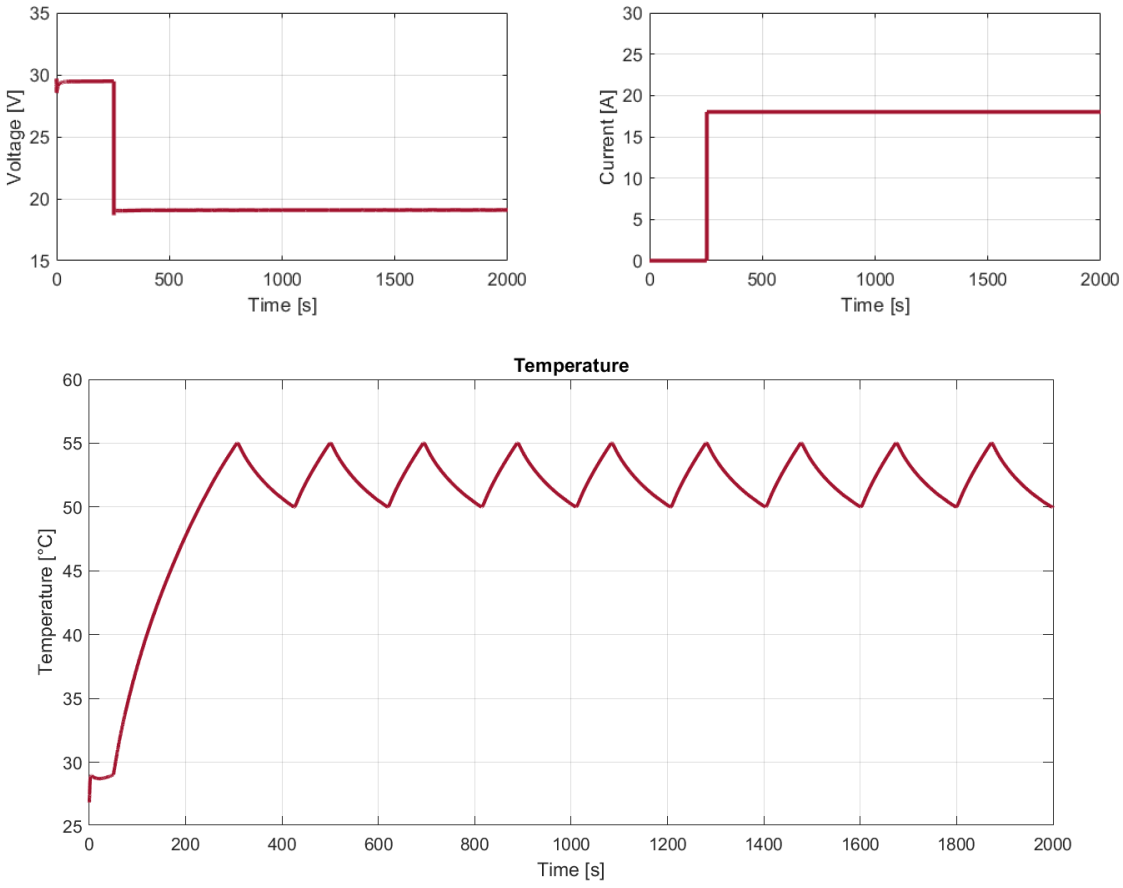

Figure 3.9: Run 1. Current and voltage (above). Temperature (below)

The test with the input ramp input is presented in figure 3.10. As the current increase, the voltage drops gradually. Clearly the temperature raise

is slower with respect to the first run. According to the model, above 20 A the cooling system is not able anymore to keep the temperature below 55°C.

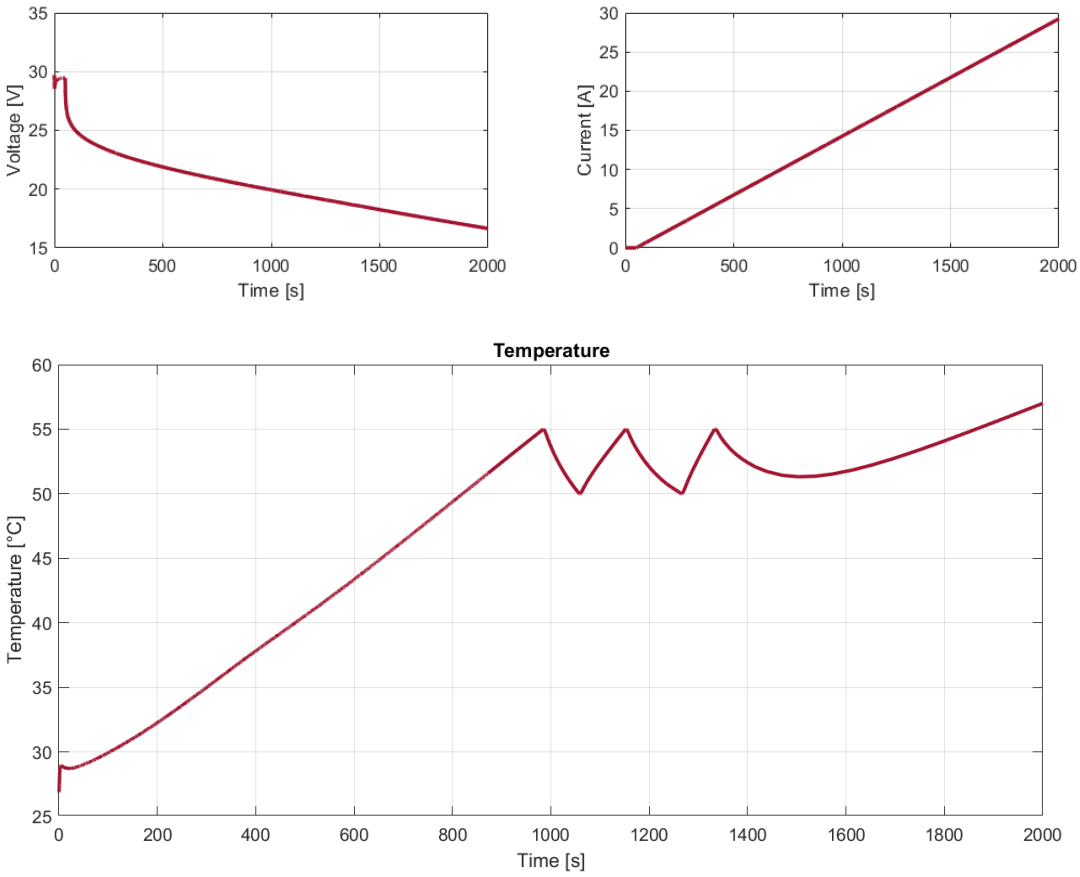

Figure 3.10: Run 2. Current and voltage (above). Temperature (below)

At this point of the work, a validation of the model is made made by comparing its result to the experimental tests performed. The electrical behaviour of the model is evaluated by comparing the polarization curves. In figure 3.11 it can be observed that the model fits pretty well the polarization curve of the actual stack, at least in a range between 0A and 18A.

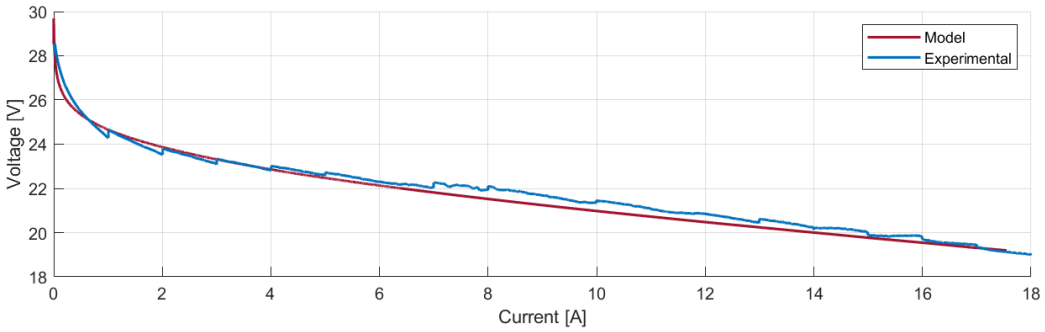

Figure 3.11: Comparison between the polarization curve estimated by the model and the experimental one

Another validation is performed by analyzing the thermal transient behaviour when the stack is subjected to the same load and conditions of the dynamic test 3 (see paragraph 4.3). As it can be seen in the figure 3.13, the thermal response of the model is a bit faster than the experimental one, maybe this is due to a difference between the assumed specific heat or mass with the real one. The equilibrium temperature is almost the same, this means that the radiator exchanger model dissipates the same amount of heat of the real one.

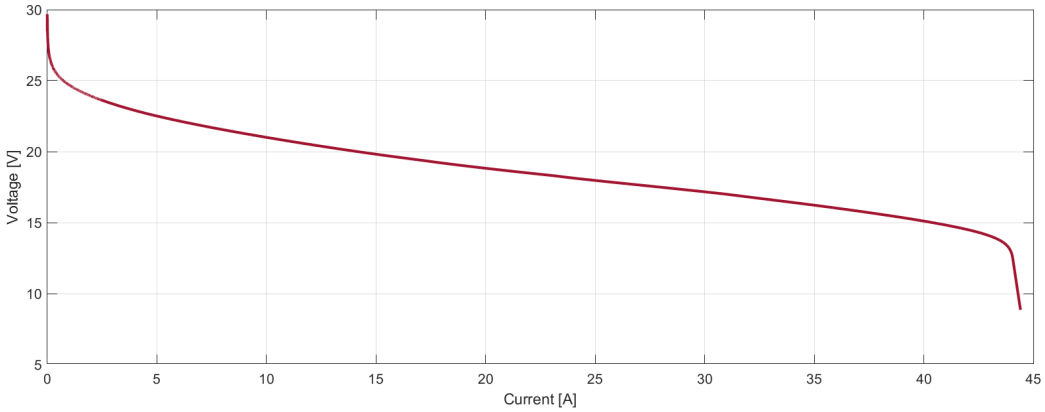

Figure 3.12: Model's polarization curve.

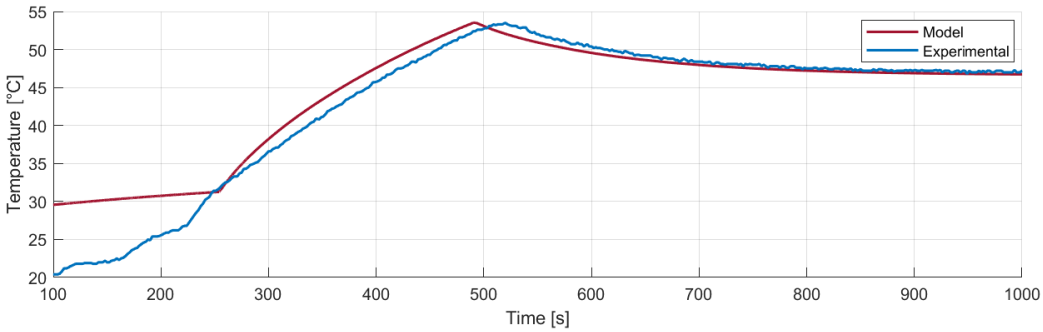

Figure 3.13: Comparison between the temperature estimated by the model and the experimental one in a test with 18 A current and fan swithced on

Another validation of the thermal modelling is performed by having a ramp between 0 and 18 A as current input. The experimental outputs are obtained by the static characterization test number three (see paragraph 4.2). The comparison between simulation and real behaviour is represented in figure 3.14. The temperature difference in the first section is present because the output temperature of the model is the actual stack temperature, while the output of the test is the stack outlet coolant temperature. As the pump starts working (at 3A current the pump is switched on), the thermocouple sense the real estimation of the stack's temperature. Some phase displacement are present especially in the section where the fan is activated, this is probably caused, again, by a mismatch in the systems parameters or by an imperfect control of temperature by the ECU. Indeed, as it can be seen, the peaks of temperature have different values, this brings to a phase displacement of the temperature oscillations.

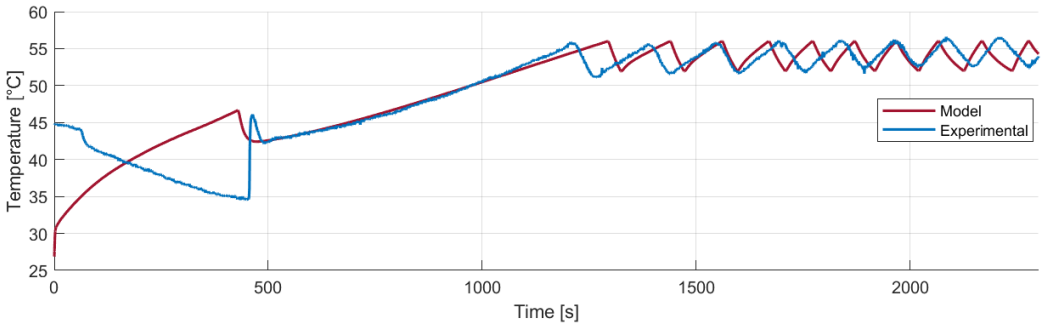

Figure 3.14: Comparison between the temperature estimated by the model and the experimental one in a test with 18 A current and fan swithced on

Chapter 4

Experimental results

4.1 System Description

The test bench is composed by the following elements:

- Fuel cell stack;
- Electronic Control Unit (ECU);
- Electronic load;
- Cooling systems;
- Sensors and acquisition system;

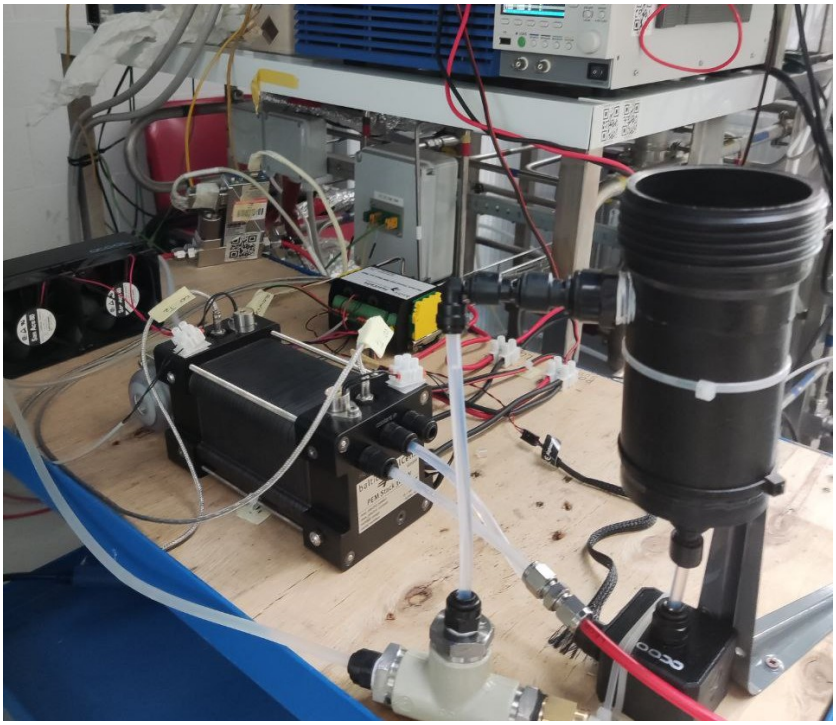

Figure 4.1: Test bench

4.1.1 Fuel Cell stack

The stack in the system is shown in figure 4.4.

Figure 4.2: Fuel Cell stack

With the stack, other auxiliary elements are present, such as pressure

regulation valve, an intake blower for air, and hydrogen exhaust condenser. Some technical specifications of the product are summed in table 4.1:

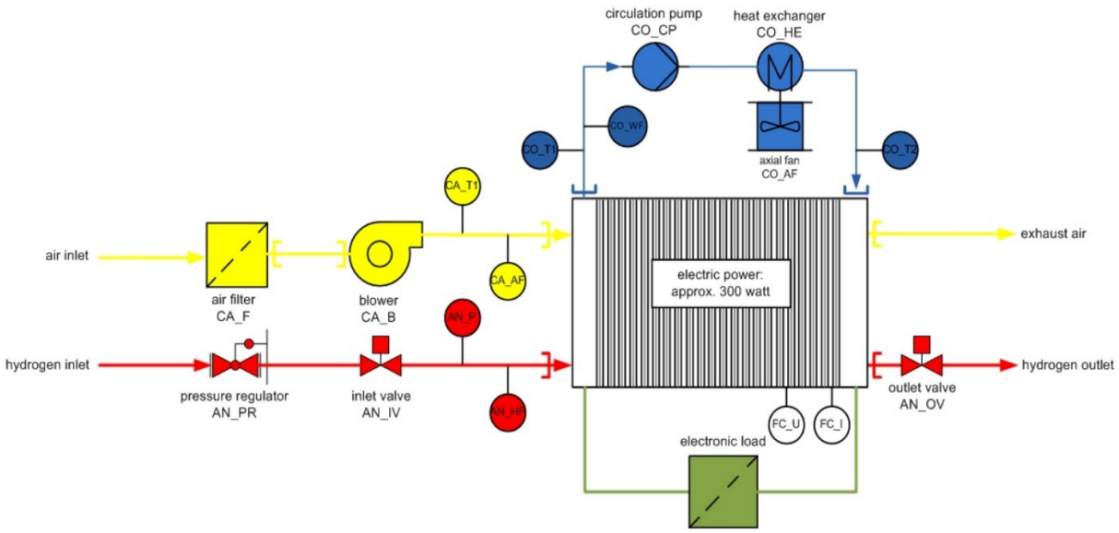

Figure 4.3: Fuel Cell stack scheme

Performance specification	Value
Voltage	15-30 V
Output	300 W
Current	18 A
Efficiency	45 %
Working temperature	50°C

Table 4.1: Stack technical specifications

4.1.2 ECU

The Electronic Control Unit (ECU) is one of the most important element in the entire system. The connection is made by serial port, from which command are sent and received.

Figure 4.4: Electronic control unit

The ECU controls and regulates the peripheral components that are required to operate the stack and measures different physical parameters. Technical specifications are in table 4.2 and a scheme of the connection of the sensors and actuator is in fig. 4.5 :

Input Voltage	12 V
Minimum currrent	5 A

Serial port settings	
Baud rate	115200
Data bits	8
Stop bits	1
Parity	None

Table 4.2: ECU technical specifications

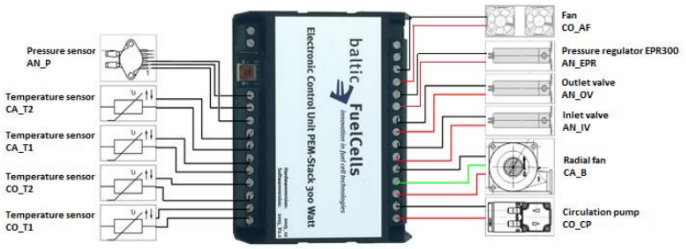

Figure 4.5: ECU scheme

4.1.3 Cooling system

The cooling system consists of elements such as a pump, radiator with fans, coolant tank, and a control system (in the ECU) that monitors and maintains the stack below the maximum allowable temperature through temperature sensors. The radiator is an "Alphacool NexXxoS XT45" model. All main parts of the radiator are made from copper.

Figure 4.6: Alphacool radiator

Fundamental technical specification of the radiator, such as heat exchange area and heat transfer coefficient, are not given. So test and characterization are necessary [see paragraph 4.3]. The circulation pump model is the "Eisstation DC-LT – Solo Top". It is very compact and has low power con-

supmtion.

Figure 4.7: Alphacool pump

In the following table some of its technical specifications:

Technical specifications	
Width	50.62 mm
Length	50.62 mm
Power	5 W
Voltage	12 V
Current	0.5 A

Table 4.3: Coolant pump technical specifications

The mass flow rate sent by the pump is not known and, given a fixed power, it depends on the pressure losses in the circuit and a measure on the test bench needs to be performed.

4.1.4 Acquisition System

To measure the characteristics of the fuel cell stack, the multi-functional electronic load "Kikusui PLZ-5W/5WZ Series" has been used. The load has been set to constant current mode (slew rate $4\frac{A}{\mu s}$), so a current value is specified and the current is kept constant even when the voltage changes. By serial port, a sequence of predetermined values is communicated to the load, this means that different steps are programmed, each one consisting of time duration and type (step or ramp) of the current. In order to do so, the software Wavy has been employed.

Figure 4.8: Electronic load

The software Wavy aids in generating and managing input sequences for the electronic load. It makes and modify sequences easily with a a user-friendly interface. Additionally, it provides a real-time monitor function that enables monitoring, logging and saving of values of voltage and current.

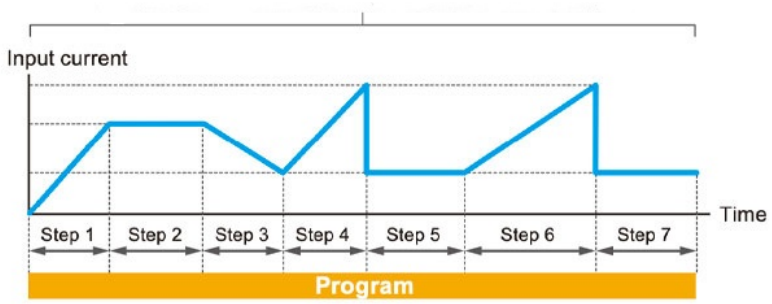

Figure 4.9: Input programming interface

Tha mass flow rate sensor is the "Bronkhorst EL-FLOW", a digital gas mass flow rate controller. It has a thermal flow rate controller and can operate between 0 and 4 bar of pressure.

Figure 4.10: Flow rate controller

The communication with the ECU is made by serial port, and it is useful to get the measurement and save them in a file with a remote terminal. In order to do so a Raspberry Pi, connected with wi-fi on a PC, has been employed. This system can not only get the measurement remotely, for example while the PEMF system is mounted on the bike, but it permits also an easy switch on/off system with a key/switch and in general it opens the possibility to create a dedicate embedded system.

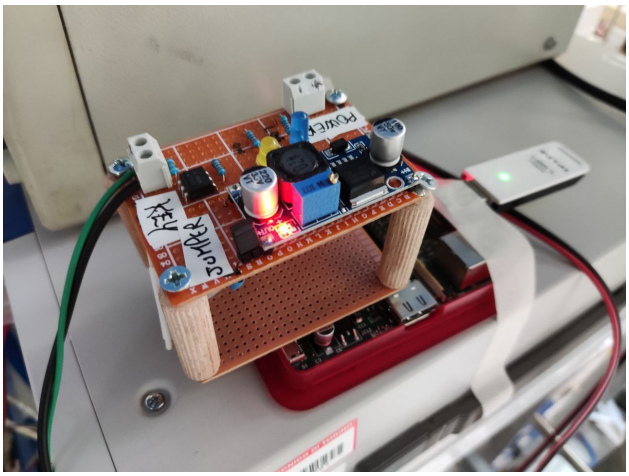

Figure 4.11: Raspberry Pi power supply circuit

Raspberry is a computer with ARM architecture on which the Linux operating system is installed. Its peculiarity is to have an integrated GPIO

(PIN) circuit with which external commands can be interfaced. The Pins operate between 0 and 3.3 V, realizing serial ports that allows you to communicate with instruments and equipment. To set up communication, it has been created a Python script that sends commands to the ECU via serial ports.

To avoid over-voltage and damaging of the Raspberry, the input circuit is coupled with the latter using a photo-transistor. The photo-transistor is connected on one side to the power supply circuit of the Raspberry Pi, and on the other side to a switch as shown in the circuit.

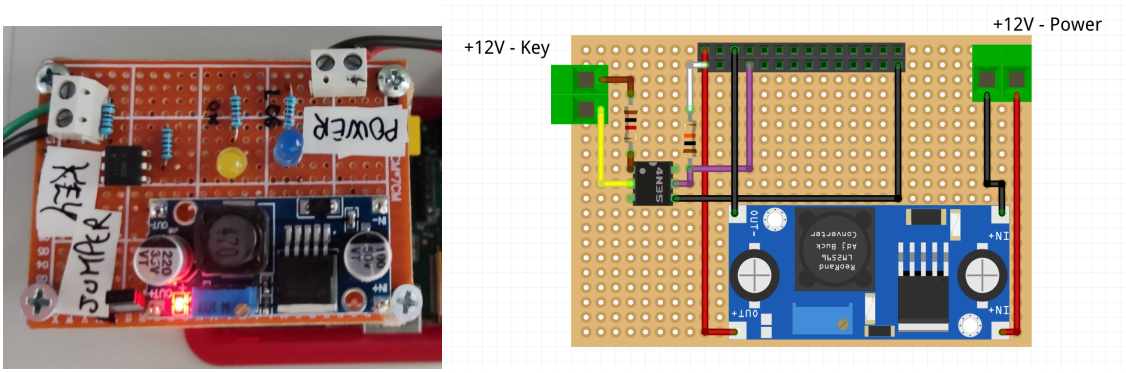

(a) Real circuit **(b)** Digitalized circuit

Figure 4.12: Power supply circuit

When the switch is active, the photo-transistor keeps the Raspberry Pi's control PIN in a voltage state. On the other hand, when the switch is deactivated, the circuit is connected to the ground, canceling the voltage. This allows the Raspberry Pi to receive a signal and, through a small Python script, send to the ECU through the serial port the command to turn the stack on or off. When the temperature reaches 55°C, the radiator's fan start blowing and a rapid decrease of temperature can be noticed. The ECU measure the stack's current and voltage, the gas pressures, the temperature of the cooling fluid at inlet/outlet of the stack and at the outlet of the radiator coolant fluid and air.

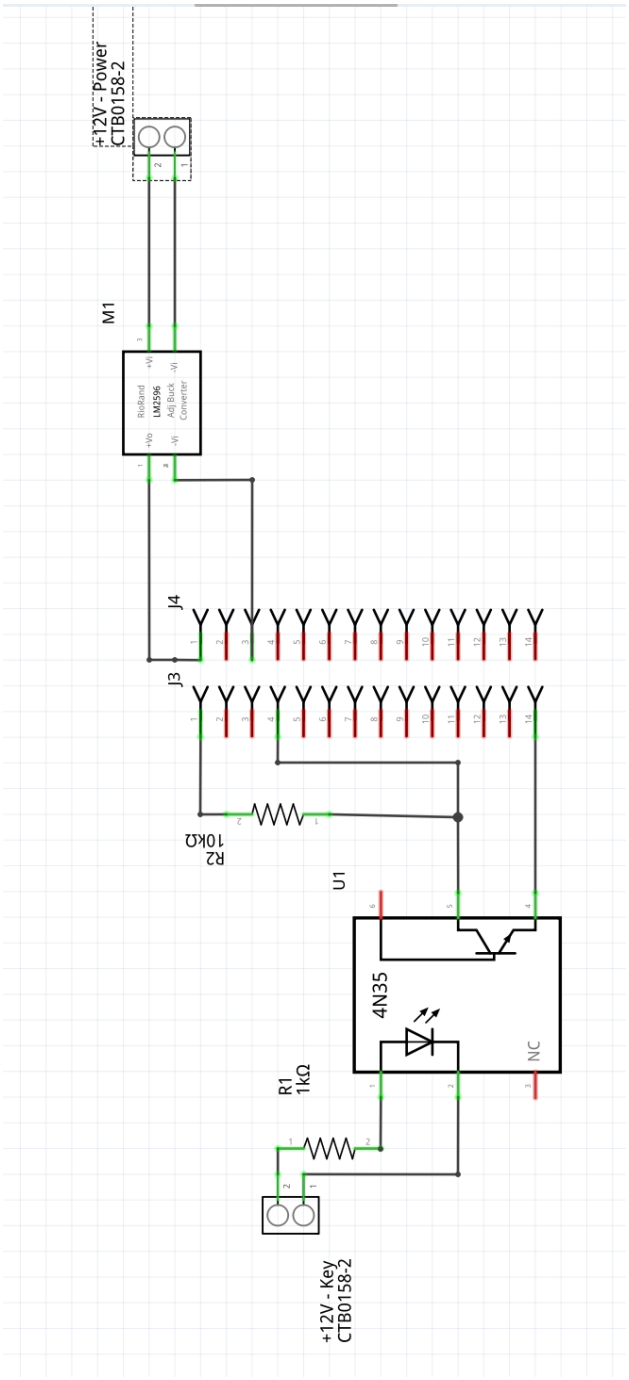

Figure 4.13: Raspberry Pi and photo-transistor

4.2 Static characterization

The first step is the evaluation of the fuel cell functionality. The characterization is necessary to check if the PEM stack suits the characteristics declared by the supplier, if it works properly and if it fits our design goals. In order to do so, different tests are performed:

1. Ramp-step current input from 0A to 10 A (Low temperature).
2. Ramp-step current input from 0A to 10 A (High temperature).
3. Ramp-step current input from 0A to 18 A and down from 18 to 0 A.

In figure 4.14, voltage, current and temperatures of the first two tests are represented. By looking at the temperature behaviour at about 450 s there is a peak, this is due to the activation of the coolant circulation pump. When the current reaches 3A, the pump is activated and the hot water inside the stack starts flowing through the temperature sensors at the inlet/outlet of the stack's coolant channels. In figure 4.15 the flow rates and the polarization curve of the stack. Despite the higher temperature, the stack performed worse in the second test, a hypothesis might be that this behaviour is due to a lack of hydrogen flow (as represented by the little under-estimation of the measured flow rate with respect to the theoretical one) maybe caused by low inlet hydrogen pressure. Another hypothesis is that there could be a flooding phenomenon inside the stack caused by an incorrect mounting of the anode/cathode exhaust channels.

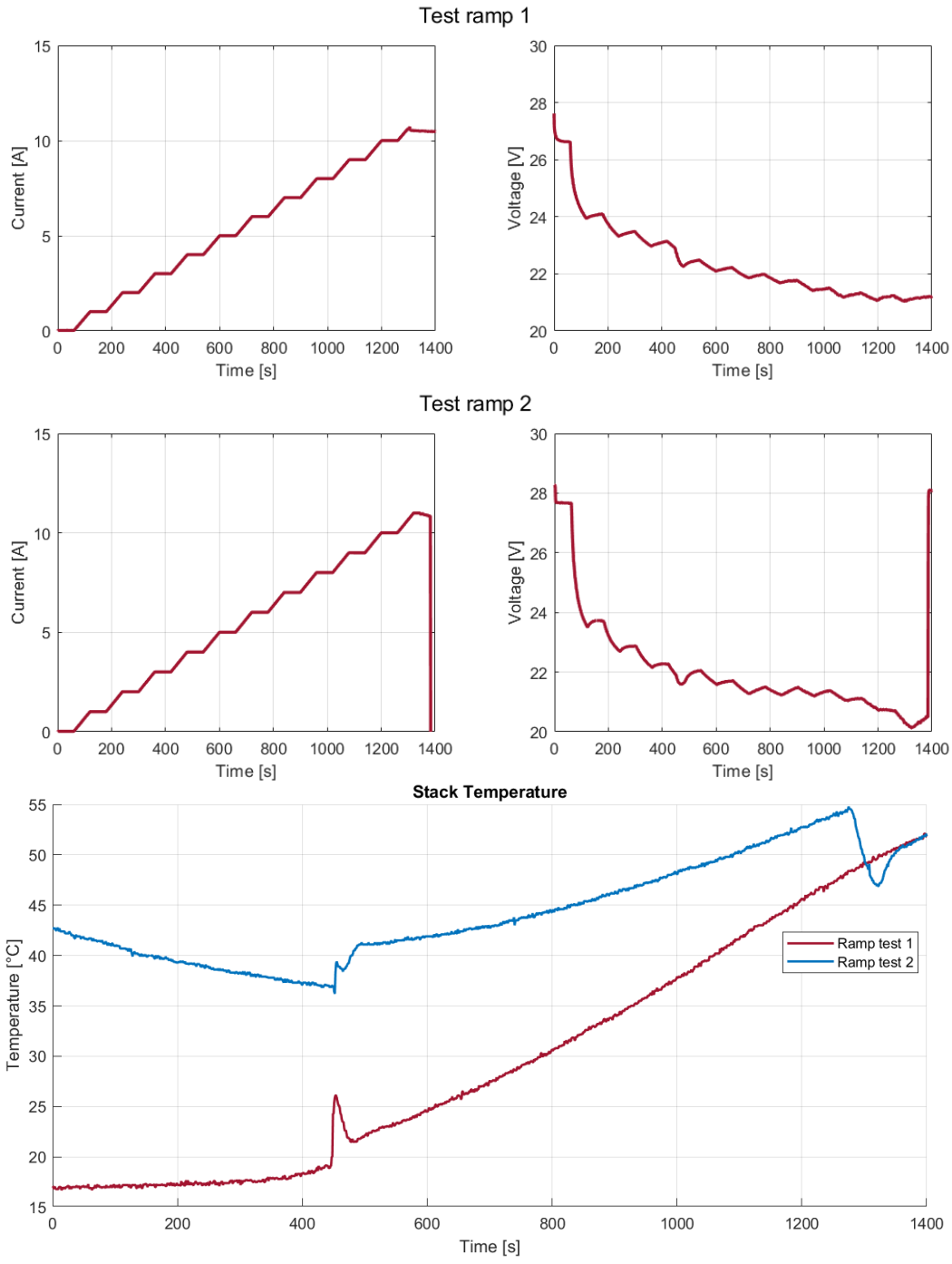

Figure 4.14: Test 1 and 2. Ramp at low and high T

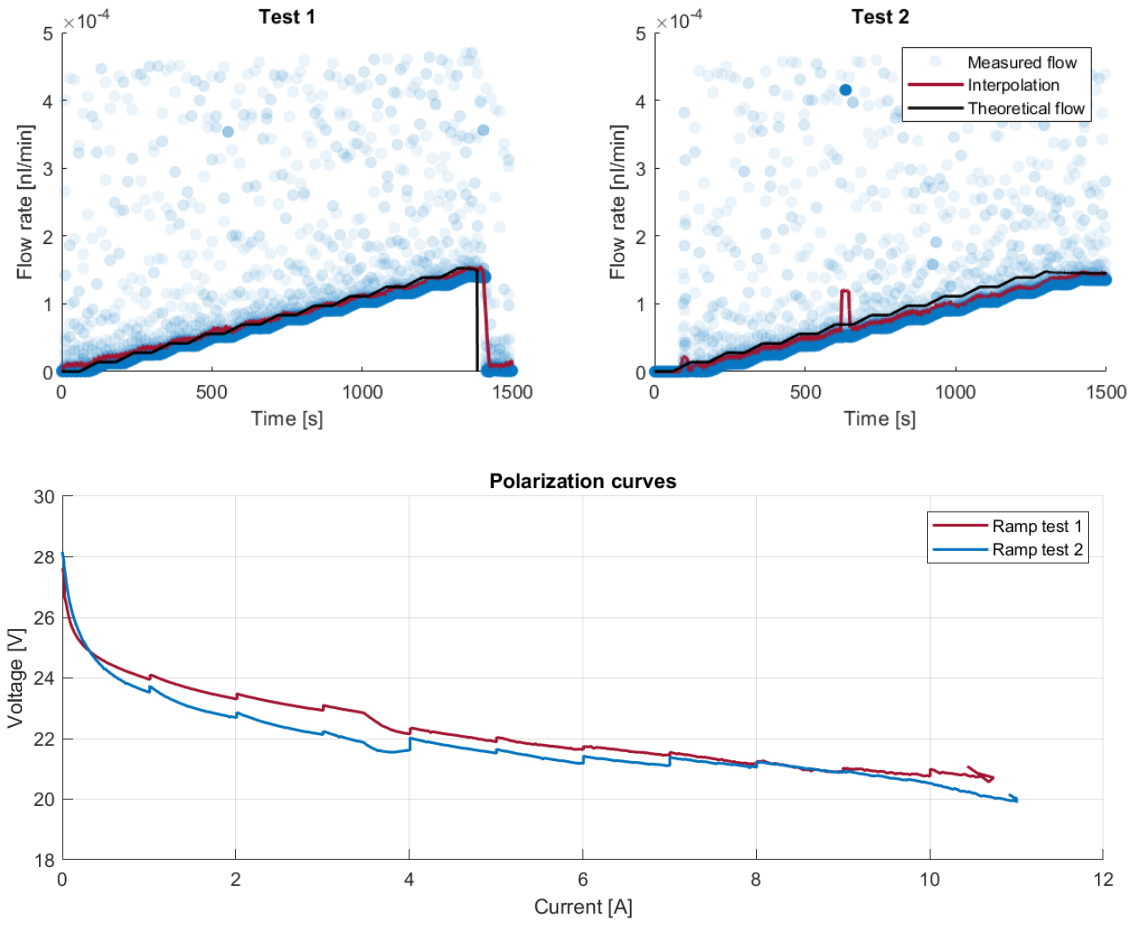

Figure 4.15: Test 1 and 2. Flow rates (above), Polarization curve (below)

Finally the static characterization is performed by increasing the current till the maximum allowed according to data-sheet (18 A) and then decreasing it to zero. In the figure 4.16 the polarization curve of the going-down current portion is higher than the increasing one. This is due to the higher temperature of the stack. Again, because of the activation of the coolant pump at about 450s, the temperature of the coolant outlet channel suddenly increase. The up and down behaviour of the temperature is caused by the activation of the radiator's fan for which the cut on/off temperatures are set respectively at 55-50 °C.

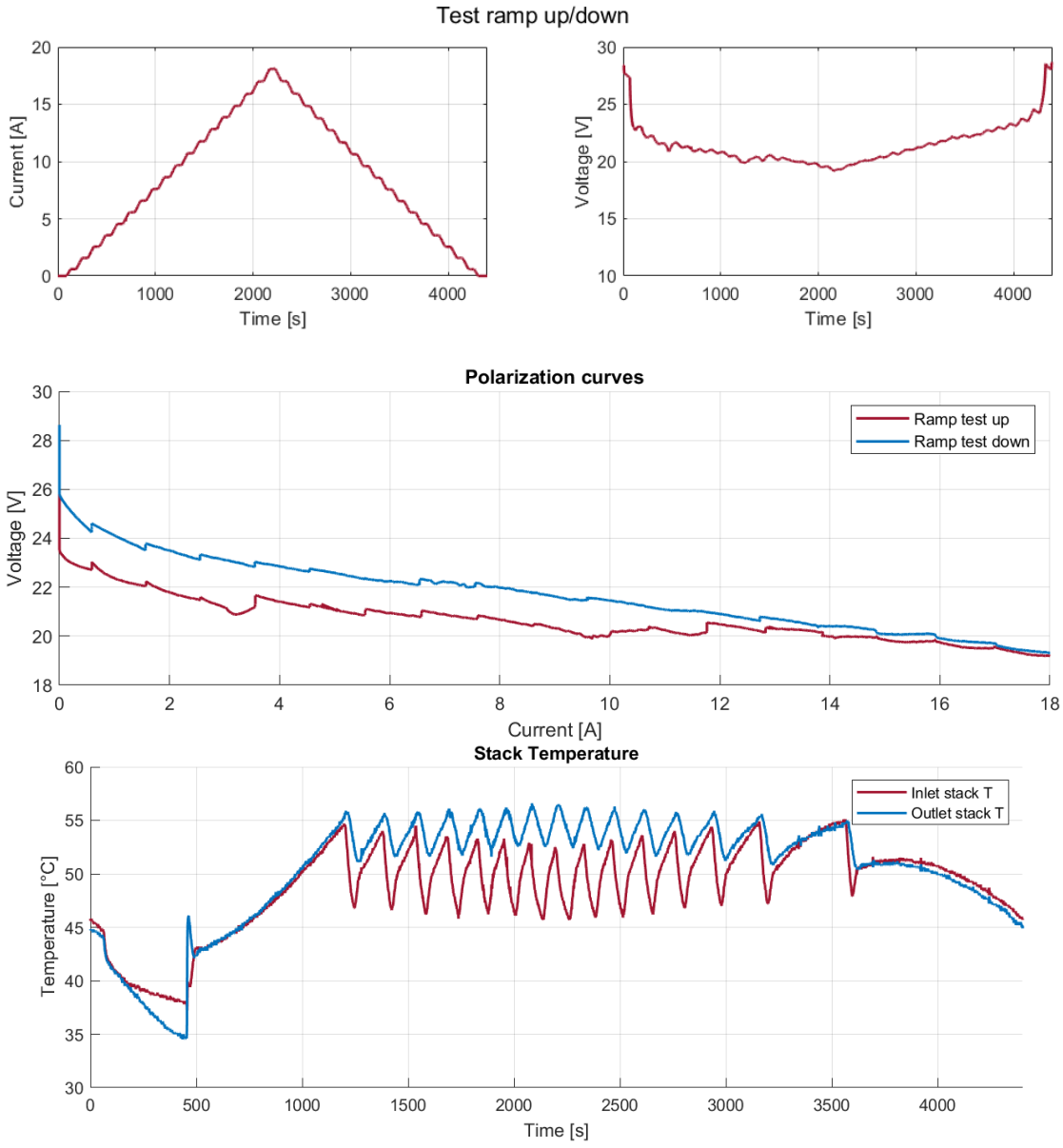

Figure 4.16: Test 3. Current, Voltage (above). Polarization curve (middle). Coolant inlet/outlet temperatures (below)

A comparison between the measure done by the ECU and the electronic load is made (fig. 4.17). The electronic load read a slightly lower voltage, probably do to the ohmic losses of the wires connecting the stack to the load's

clamp. For the future tests, this problem is avoided by connecting the wires to other clamps of the electronic load in a "4-wire" configuration.

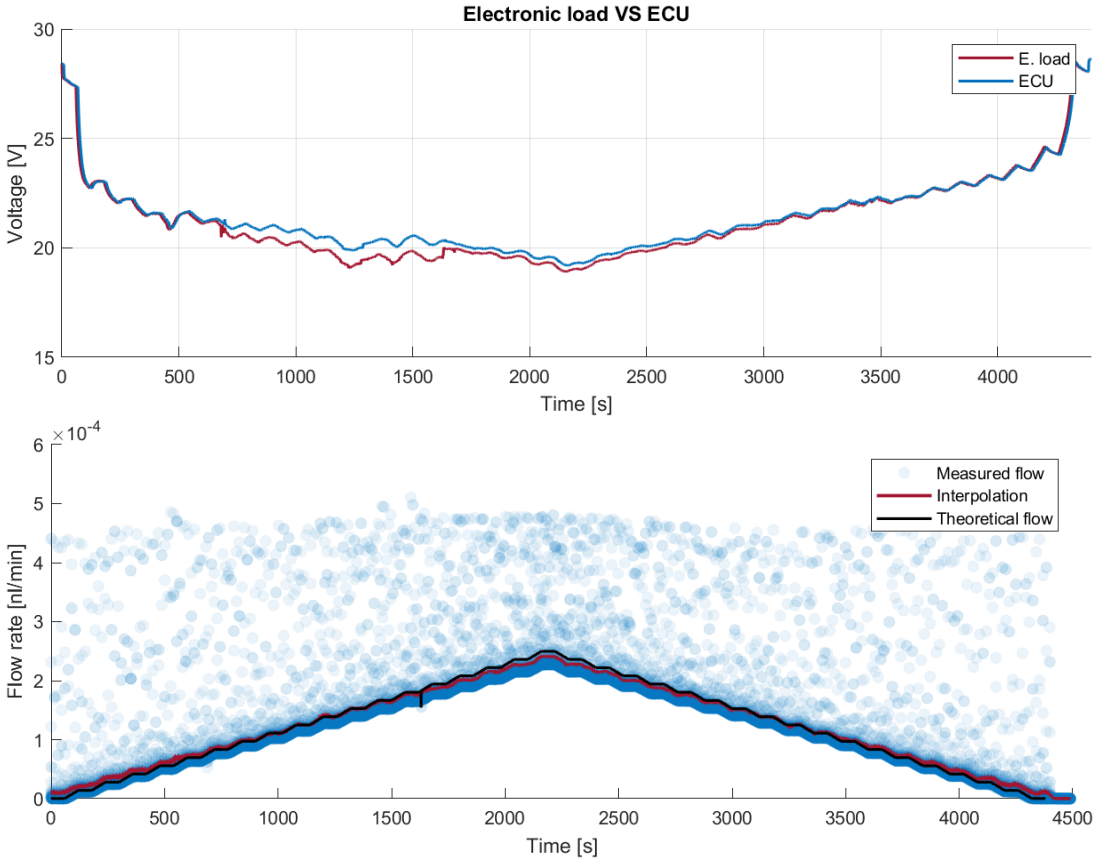

Figure 4.17: Test 3. ECU vs Electronica load (above). Flow rate (below)

4.3 Dynamic characterization

The dynamic characterization is made by sending as input different current steps in order to see how the stack behave with a sudden increase/decrease of electrical demand. The test performed are:

1. Dynamic test from 0 to 15 A with pre-heating.
2. Dynamic test from 0 to 15 A withe pre-heating and DC-DC converter.
3. Thermal characterization with steps from 0 to 18A and fan swithed on.

In the dynamic test is firstly performed a pre-heating of the stack in order to avoid damages of the cells. This is made by gradually setting the current to a high value (15-18A). In fig. 4.18 it can be observed an undershoot or overshoot of the voltage as the current jumps widely from a step to another. This is because the mass transfer is slower than the electro-chemical reaction: by increasing the current demand, the water generation rate and the gas consumption increase too. The water starts accumulating in the GDL and the reactants are in this way blocked causing a sudden starvation. A constant value of the voltage is achieved again as soon as a new equilibrium of the mass transfer is reached. On the other side, when the current decrease, the gas consumption rate decrease but the oxygen concentration is high, this brings to an over-voltage [57] [58]. This phenomenon can be observed in the other dynamic tests too. Again in figure 4.18 it can be seen that the temperature during the dynamic input becomes unstable, with the inlet stack temperature overcoming the outlet one. This is caused by the fact that at 0A, the coolant pump stops and this makes the thermometer measure intermittently the real stack temperature.

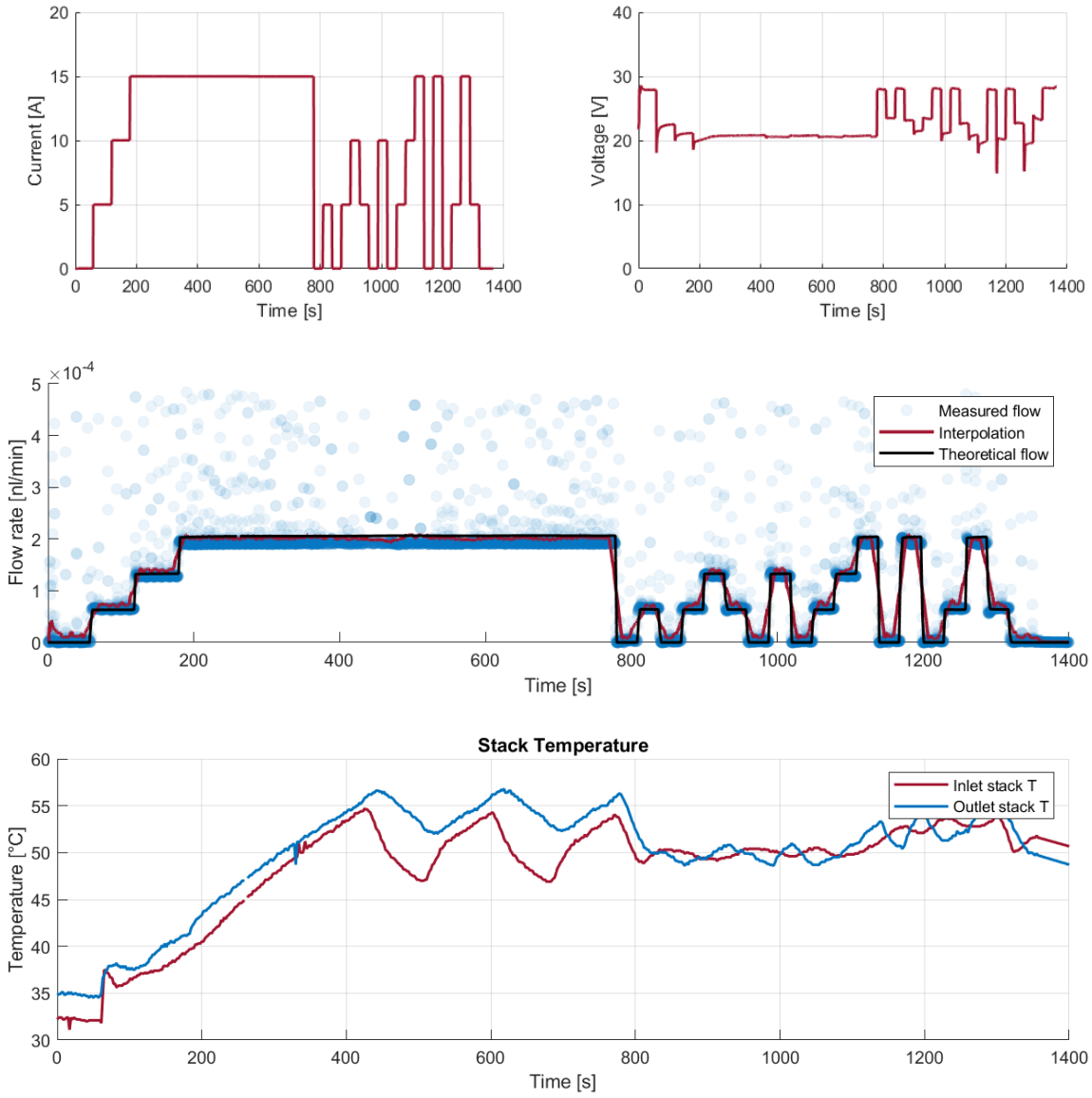

Figure 4.18: Dynamic test 1. Current and voltage (above). Flow rate(middle). Temperature (below)

The second test is made by connecting a DC-DC converter in series with stack. The converter is used to keep a constant voltage value across the electronic load. This value is set at 36V. In figure 4.18 are represented

the flow rate and the coolant stack inlet/outlet temperatures, and the same considerations of the first test can be made. In the figure 4.19 it can be seen how the DC-DC converter reacts to the sudden current changes. It can be noticed that as the current demand suddenly increase and the undershoot of the voltage occurs, the converter fails to keep the voltage constant, this is a common issue when dealing with variable load in a DC-DC converter. This results also in a higher current sent by the device.

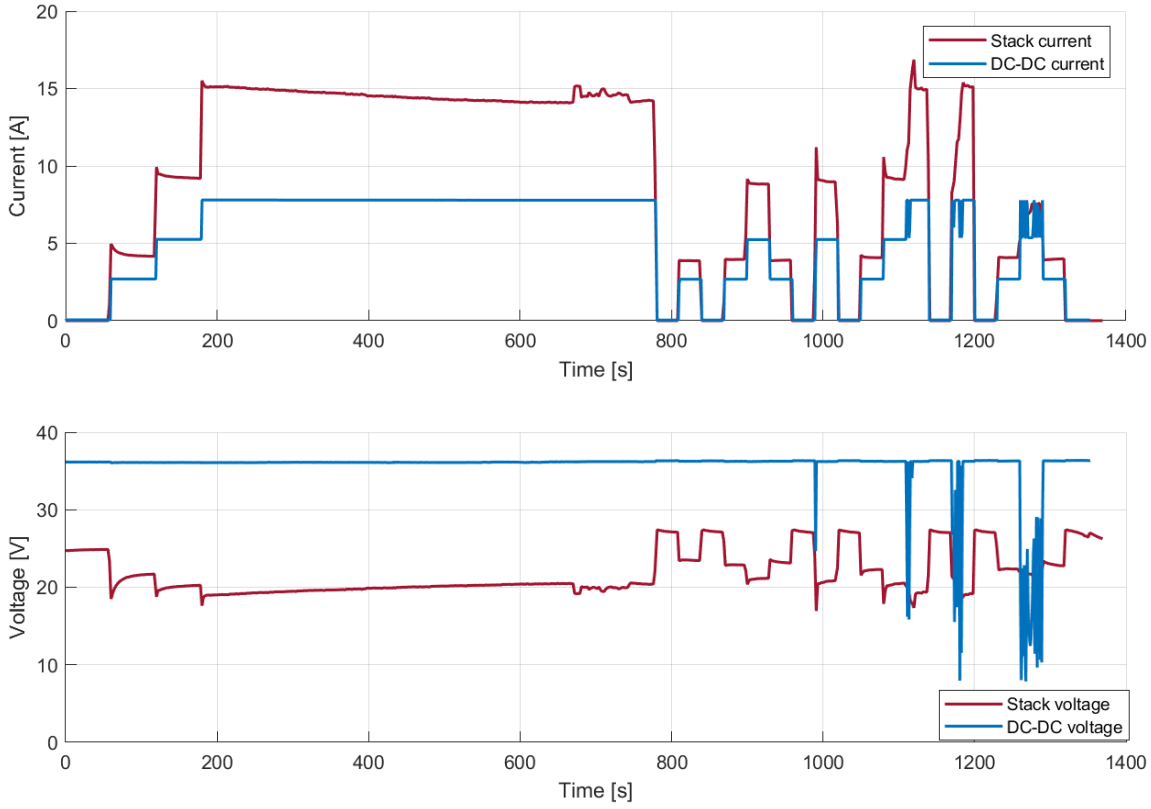

Figure 4.19: Test 2. Stack vs electronic load current (above). Stack vs electronic load voltage (below)

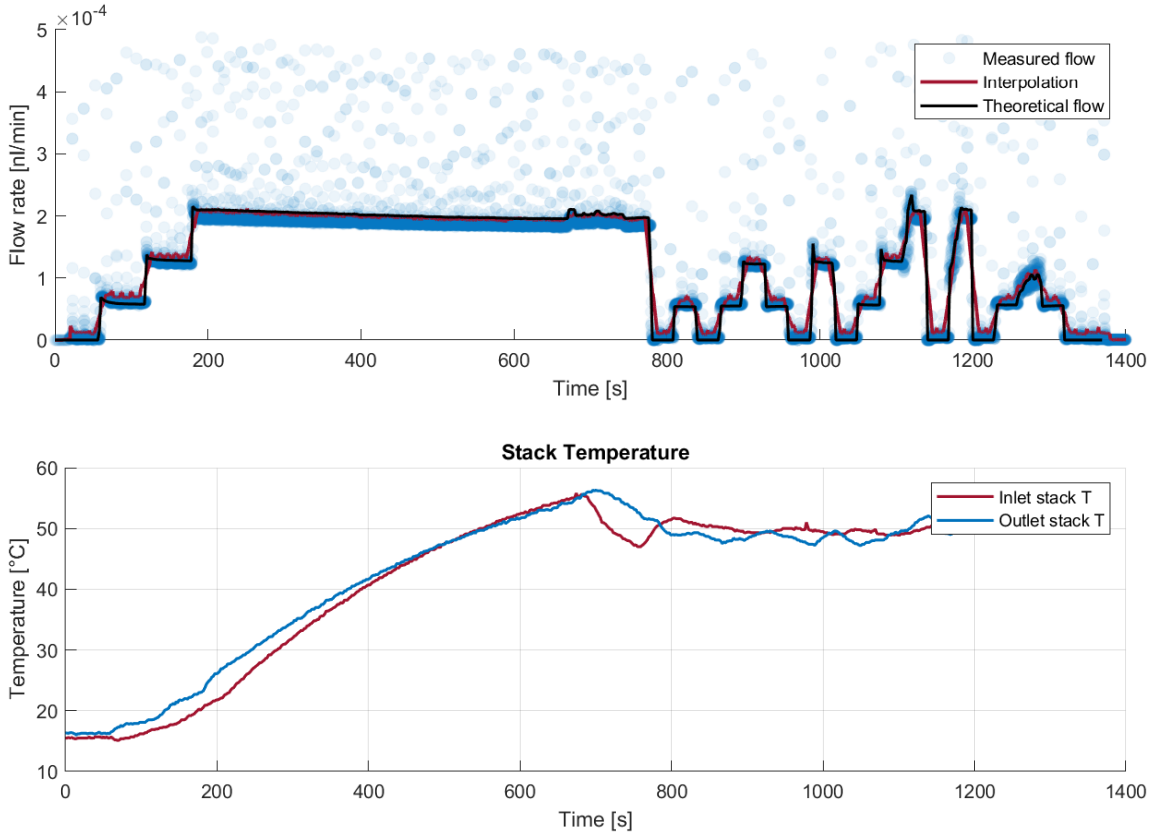

Figure 4.20: Test 2. Flow rate (above). Temperatures (below)

The third test is made heating up the stack by setting the working conditions to the maximum power (18A). When the temperature reached 54°C, the radiator's blower is activated till the equilibrium temperature of the stack is achieved.In the figure 4.21 the voltages under/over-shooting already seen in the other tests can be noticed and also a slightly increase of the voltage between the seconds 250 and 480 (18A step) can be observed, followed by a decrease due to the activation of the fan resulting in a cool-down of the stack. A closer view of the transient response is also highlighted, showing that the stack reacts with a delay from 0.5 to 1 seconds with the respect to the given current input.

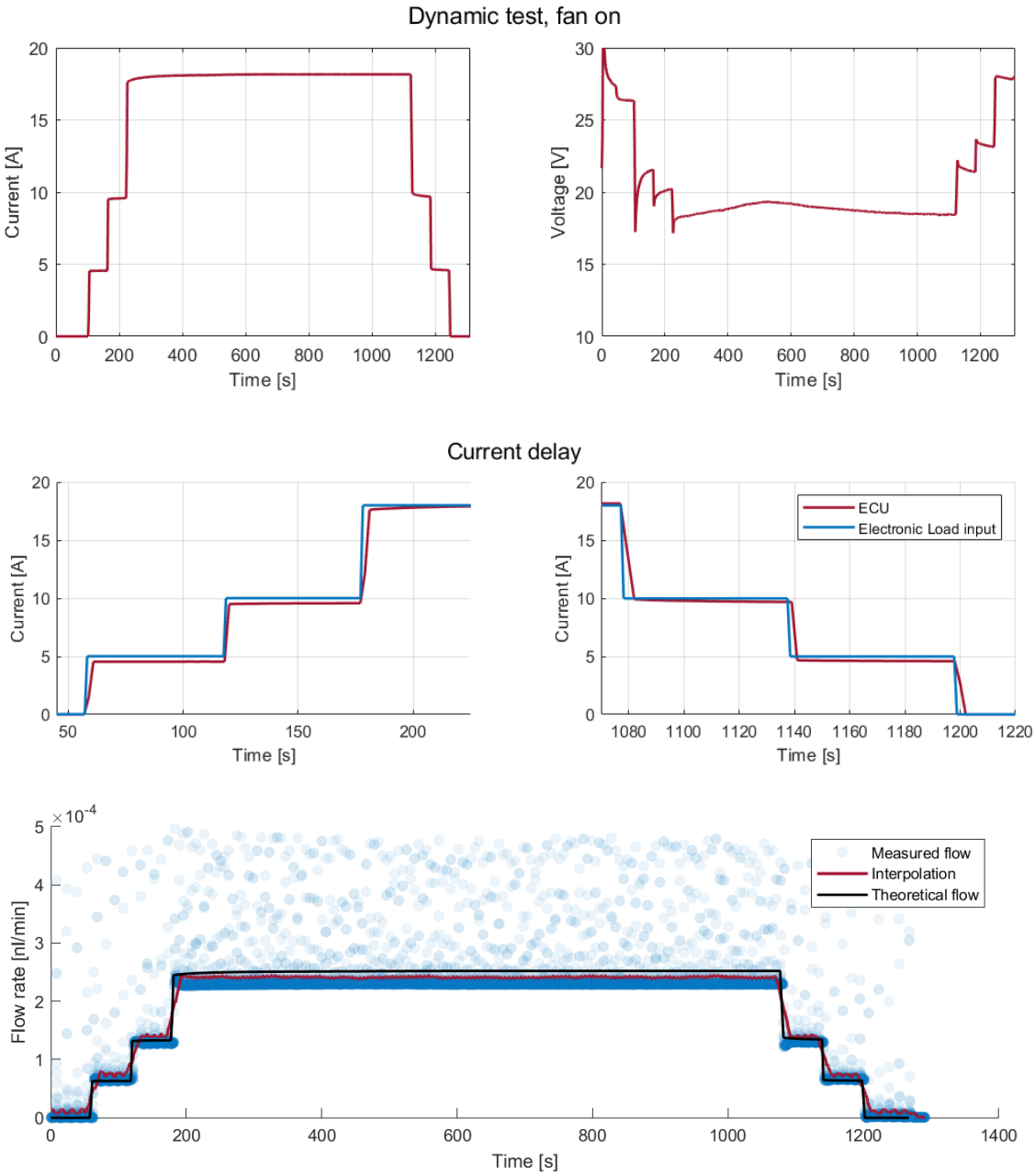

Figure 4.21: Dynamic test 3. Current and voltage (above). Detail of the stack vs electronic load current (middle). Flow rate (below)

As it can be seen in figure 4.22, the temperature of the stack increases till the activation of the radiator's fan which is kept on till the reaching of the equilibrium temperature. This test is used to characterize the thermal system, and the calculations are performed when the steady state is reached, as no transient oscillations occur. The heat produced by the stack is evaluated as follow:

$$Q_{stack} = \dot{m}_{cool} c_p (T_{out} - T_{in}) \tag{4.1}$$

Where T_{out} and T_{in} are the outlet and inlet temperature of the stack's coolant channel, c_p is the coolant specific heat and $\dot{m}_{cool}$ is the coolant mass flow rate (measured). The air flow rate can be calculated as:

$$\dot{m}_{air} = \frac{Q_{diss}}{c_{p,air}(T_{air,out} - T_{air,amb})} \tag{4.2}$$

Where $T_{air,out}$ is the air outlet temperature $T_{air,amb}$ is the ambient temperature, $c_{p,air}$ is the air specific heat and Q_{diss} is the heat dissipated by the radiator:

$$Q_{diss} = \dot{m}_{cool} c_p (T_{rad,in} - T_{rad,out}) \tag{4.3}$$

In order to get the thermal resistivity of the exchanger, the logarithmic mean temperature difference (LMTD) method is used. According to this method the product of the heat transfer coefficient and the exchange area is:

$$U\ A = \frac{Q_{diss}}{LMTD} \tag{4.4}$$

Where LMTD is evaluated as follow:

$$LMTD = \frac{\Delta T_A - \Delta T_B}{ln \frac{\Delta T_A}{\Delta T_B}} \tag{4.5}$$

ΔT_A and ΔT_B are the inlet and outlet temperature differences.

An estimation of the maximum ambient temperature in which the stack can operate can be made with effectiveness-NTU method, already seen in equation 3.78. For a cross-flow arrangement with mixed air and unmixed fluid the effectiveness is calculated as in 3.74. Considering the stack working at its maximum power and the temperature limit for the safety of the stack at 60°C, the maximum ambient temperature is:

$$T_{max,amb} = T_{max} - \frac{Q_{stack,max}}{\epsilon \dot{m}_{air} c_{p,air}} \tag{4.6}$$

The parameters evaluated at steady-state are:

Coolant specific heat (water)	4186 $\frac{J}{kgK}$
Air specific heat	1005 $\frac{J}{kgK}$
Ambient temperature	23 °C
Air outlet equilibrium temperature	31.5 °C
Stack equilibrium temperature	47 °C
Stack maximum heat produced	430 W
Radiator heat dissipated	383 W
Thermal resistance	0.0345 $\frac{K}{W}$
Maximum ambient temperature	37 °C

Table 4.4: Experimentally evaluated parameters

In figure 4.22 and 4.23 are represented the heat produced by the stack and the heat dissipated by the radiator. When the stack is increasing its temperature during the load at 18A, the heat goes down and then up again reaching an equilibrium level . This happens because of the transient change of inlet and outlet temperatures, with the thermocouples measuring the increase of the inlet fluid temperature before the outlet one. Actually the stack produces the same heat as the one of the equilibrium.

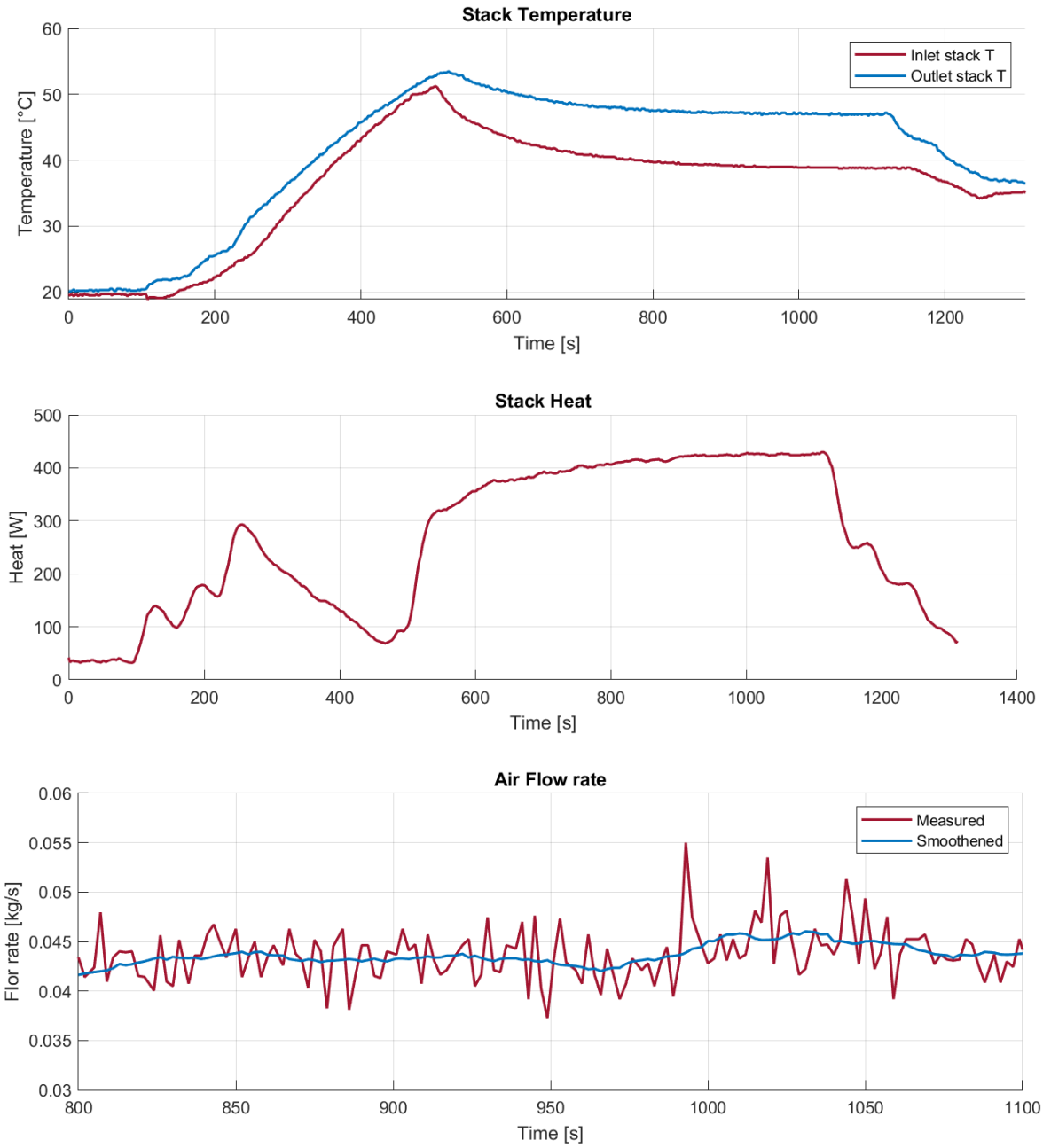

Figure 4.22: Dynamic test 3. Temperature (above). Heat produced by the stack (middle). Air mass flow rate sent by the radiator's fan (below)

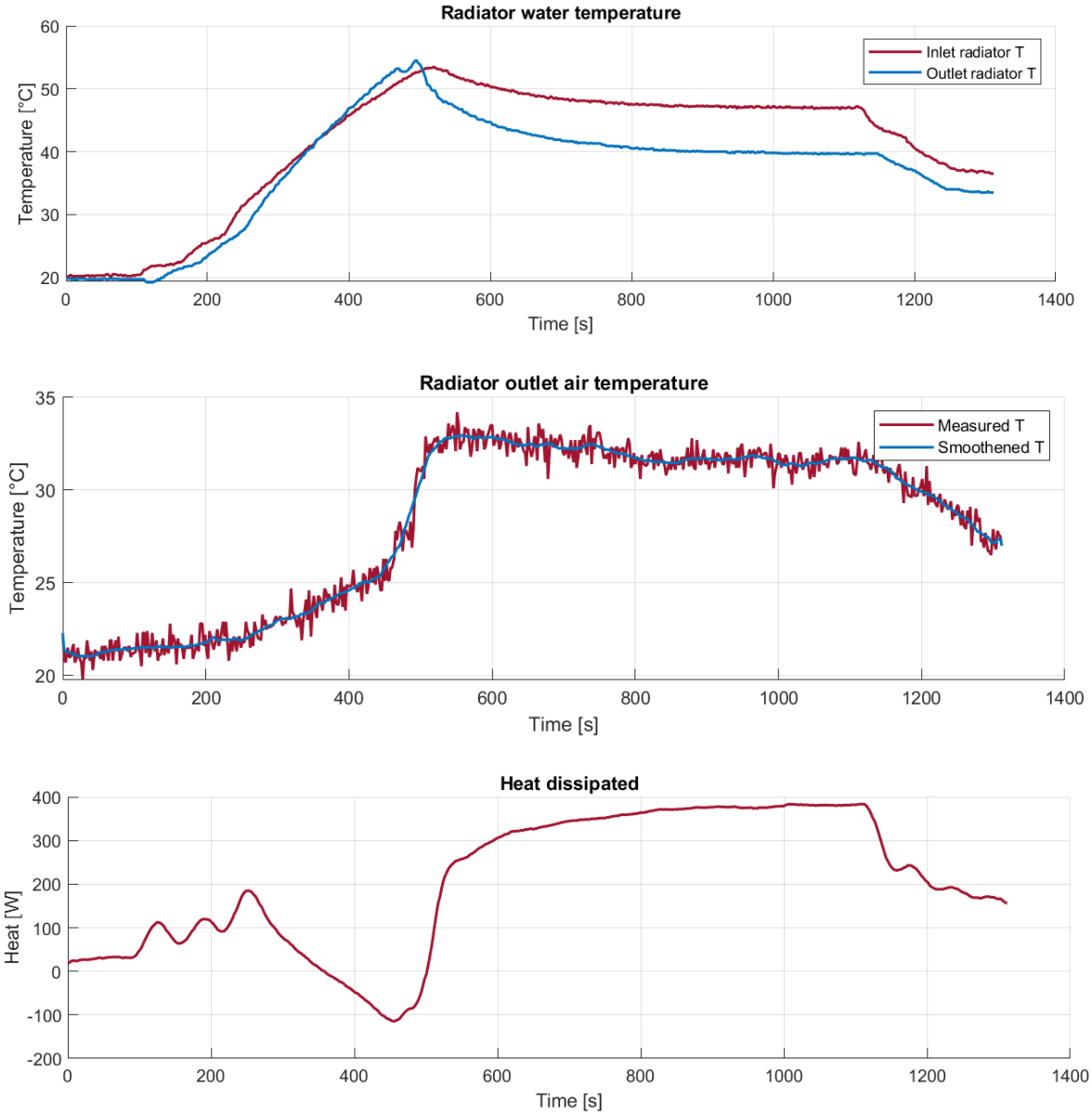

Figure 4.23: Dynamic test 3. Temperature (above). Heat produced by the stack (middle). Air mass flow rate sent by the radiator's fan (below)

Chapter 5

Conclusions And Future Works

The aim of this study is the realization of a preliminary design for a e-cargo bike's PEMFC system in a hybrid configuration with a battery pack. The focus of the thesis is thermal management part of the design, and the work is divided into two parts. The first part is the creation and the validation of a PEMFC system model on a Simscape/Simulink environment. The second part is the experimental evaluation of the components which are going to be mounted on the bike. The system is composed by a stack, a coolant pump, an air-water heat exchanger with fan and the hydrogen source.

The tests carried out on the stack have shown the cell performance's adherence to the ones communicated by the supplier, that the stack satisfies the power demand assumed in the design phase if the load is stable enough, and that the cooling system is capable to guarantee the safety conditions at any load.

The validation of the model is made by comparing the output of the simulation with the experimental parts just cited. The model fits well the electrical behaviour and the power output of the real stack while the thermal behaviour is not perfectly comparable to the measurements, probably due to the parameters assumed or took from literature which are not exactly the same of the system tested. Another problem of the model is related to the hydrogen source section which has to be modified in order to be more similar to the real one, as no recirculation is present on the tested stack.

Further improvements need to be performed on the model and other tests are necessary. Some examples are:

1. Adjustment of the hydrogen source section;

2. Inclusion of the metal hydrides part in the model;
3. Characterization of the metal hydrides tank and consequent validation of the model;
4. General model finishing by increasing the number of input variables like a distinction between the starting stack, coolant or environment temperature;
5. Tuning of the parameters according to the experimental outputs;
6. Modelling of different cooling strategies and configurations.

Appendix A

Appendix

Bibliography

[1] Jay Tawee Pukrushpan. *Modeling and control of fuel cell systems and fuel processors*. University of Michigan, 2003.

[2] Yun Wang, Daniela Fernanda Ruiz Diaz, Ken S Chen, Zhe Wang, and Xavier Cordobes Adroher. Materials, technological status, and fundamentals of pem fuel cells–a review. *Materials today*, 32:178–203, 2020.

[3] Sharon Thomas, Marcia Zalbowitz, and Dennis Gill. Fuel cells: Green power, December 31, 2006 2006.

[4] James Larminie, Andrew Dicks, and Maurice S McDonald. *Fuel cell systems explained*, volume 2. J. Wiley Chichester, UK, 2003.

[5] Qi Li, Weirong Chen, Zhixiang Liu, Ming Li, and Lei Ma. Development of energy management system based on a power sharing strategy for a fuel cell-battery-supercapacitor hybrid tramway. *Journal of Power Sources*, 279:267–280, 2015.

[6] Jose Miguel Pasini, Bart A van Hassel, Daniel A Mosher, and Michael J Veenstra. System modeling methodology and analyses for materials-based hydrogen storage. *international journal of hydrogen energy*, 37(3):2874–2884, 2012.

[7] Christopher L Aardahl and Scot D Rassat. Overview of systems considerations for on-board chemical hydrogen storage. *International Journal of Hydrogen Energy*, 34(16):6676–6683, 2009.

[8] Jose Miguel Pasini, Claudio Corgnale, Bart A van Hassel, Theodore Motyka, Sudarshan Kumar, and Kevin L Simmons. Metal hydride material requirements for automotive hydrogen storage systems. *International journal of hydrogen energy*, 38(23):9755–9765, 2013.

[9] Djafar Chabane, Mehroze Iqbal, Fabien Harel, Abdesslem Djerdir, Denis Candusso, Omar Elkedim, and Nour-eddin Fenineche. Coupling a metal hydride tank with a pemfc for vehicular applications: A simulations framework. *International Journal of Energy Research*, 45(11):16511–16523, 2021.

[10] Guangsheng Zhang and Satish G Kandlikar. A critical review of cooling techniques in proton exchange membrane fuel cell stacks. *international journal of hydrogen energy*, 37(3):2412–2429, 2012.

[11] Mohamed HS Bargal, Mohamed AA Abdelkareem, Qi Tao, Jing Li, Jianpeng Shi, and Yiping Wang. Liquid cooling techniques in proton exchange membrane fuel cell stacks: A detailed survey. *Alexandria Engineering Journal*, 59(2):635–655, 2020.

[12] Xingqiang Zhao, Yankun Li, Zhixiang Liu, Qi Li, and Weirong Chen. Thermal management system modeling of a water-cooled proton exchange membrane fuel cell. *International Journal of Hydrogen Energy*, 40(7):3048–3056, 2015.

[13] M Secanell, K Karan, A Suleman, and N Djilali. Multi-variable optimization of pemfc cathodes using an agglomerate model. *Electrochimica Acta*, 52(22):6318–6337, 2007.

[14] Zhi-Jun Mo, Xin-Jian Zhu, Ling-Yun Wei, and Guang-Yi Cao. Parameter optimization for a pemfc model with a hybrid genetic algorithm. *International Journal of Energy Research*, 30(8):585–597, 2006.

[15] Shan-Hai Ge and Bao-Lian Yi. A mathematical model for pemfc in different flow modes. *Journal of Power Sources*, 124(1):1–11, 2003.

[16] Junbom Kim, Seong-Min Lee, Supramaniam Srinivasan, and Charles E Chamberlin. Modeling of proton exchange membrane fuel cell performance with an empirical equation. *Journal of the electrochemical society*, 142(8):2670, 1995.

[17] JJ Baschuk and Xianguo Li. Modelling of polymer electrolyte membrane fuel cells with variable degrees of water flooding. *Journal of power sources*, 86(1-2):181–196, 2000.

[18] S Shimpalee, U Beuscher, and JW Van Zee. Analysis of gdl flooding effects on pemfc performance. *Electrochimica Acta*, 52(24):6748–6754, 2007.

[19] Curtis Marr and Xianguo Li. Composition and performance modelling of catalyst layer in a proton exchange membrane fuel cell. *Journal of Power Sources*, 77(1):17–27, 1999.

[20] Horng-Wen Wu. A review of recent development: Transport and performance modeling of pem fuel cells. *Applied energy*, 165:81–106, 2016.

[21] Lei Xing, Qiong Cai, Chenxi Xu, Chunbo Liu, Keith Scott, and Yongsheng Yan. Numerical study of the effect of relative humidity and stoichiometric flow ratio on pem (proton exchange membrane) fuel cell performance with various channel lengths: An anode partial flooding modelling. *Energy*, 106:631–645, 2016.

[22] Thomas F Fuller and John Newman. Water and thermal management in solid-polymer-electrolyte fuel cells. *Journal of the Electrochemical Society*, 140(5):1218, 1993.

[23] K Dannenberg, P Ekdunge, and Göran Lindbergh. Mathematical model of the pemfc. *Journal of Applied Electrochemistry*, 30:1377–1387, 2000.

[24] D Singh, DM Lu, and N Djilali. A two-dimensional analysis of mass transport in proton exchange membrane fuel cells. *International Journal of Engineering Science*, 37(4):431–452, 1999.

[25] L Dumercy, R Glises, H Louahlia-Gualous, and JM Kauffmann. Thermal management of a pemfc stack by 3d nodal modeling. *Journal of Power Sources*, 156(1):78–84, 2006.

[26] Sandip Dutta, Sirivatch Shimpalee, and JW Van Zee. Numerical prediction of mass-exchange between cathode and anode channels in a pem fuel cell. *International Journal of Heat and Mass Transfer*, 44(11):2029–2042, 2001.

[27] Liyan Zhang, Mu Pan, and Shuhai Quan. Model predictive control of water management in pemfc. *Journal of Power Sources*, 180(1):322–329, 2008.

[28] KP Adzakpa, Julien Ramousse, Y Dubé, H Akremi, K Agbossou, M Dostie, A Poulin, and M Fournier. Transient air cooling thermal modeling of a pem fuel cell. *Journal of Power Sources*, 179(1):164–176, 2008.

[29] Kristián Ondrejička, Viktor Ferencey, and Michal Stromko. Modeling of the air-cooled pem fuel cell. *IFAC-PapersOnLine*, 52(27):98–105, 2019.

[30] Faysal Tiss, Ridha Chouikh, and Amenallah Guizani. Dynamic modeling of a pem fuel cell with temperature effects. *International journal of hydrogen energy*, 38(20):8532–8541, 2013.

[31] Elham Hosseinzadeh, Masoud Rokni, Abid Rabbani, and Henrik Hilleke Mortensen. Thermal and water management of low temperature proton exchange membrane fuel cell in fork-lift truck power system. *Applied energy*, 104:434–444, 2013.

[32] WRW Daud, RE Rosli, EH Majlan, SAA Hamid, R Mohamed, and T Husaini. Pem fuel cell system control: A review. *Renewable Energy*, 113:620–638, 2017.

[33] Jong-Woo Ahn and Song-Yul Choe. Coolant controls of a pem fuel cell system. *Journal of Power Sources*, 179(1):252–264, 2008.

[34] Claudio Corgnale, Bruce J Hardy, David A Tamburello, Stephen L Garrison, and Donald L Anton. Acceptability envelope for metal hydride-based hydrogen storage systems. *International journal of hydrogen energy*, 37(3):2812–2824, 2012.

[35] Raquel Busqué, Ricardo Torres, Joan Grau, Vicente Roda, and Attila Husar. Mathematical modeling, numerical simulation and experimental comparison of the desorption process in a metal hydride hydrogen storage system. *international journal of hydrogen energy*, 43(35):16929–16940, 2018.

[36] Ju-Hyeong Cho, Sang-Seok Yu, Man-Young Kim, Sang-Gyu Kang, Young-Duk Lee, Kook-Young Ahn, and Hyun-Jin Ji. Dynamic modeling and simulation of hydrogen supply capacity from a metal hydride tank. *International journal of hydrogen energy*, 38(21):8813–8828, 2013.

[37] Anggito P Tetuko, Bahman Shabani, and John Andrews. Thermal coupling of pem fuel cell and metal hydride hydrogen storage using heat pipes. *international journal of hydrogen energy*, 41(7):4264–4277, 2016.

[38] K Malleswararao, N Aswin, S Srinivasa Murthy, and Pradip Dutta. Performance prediction of a coupled metal hydride based thermal energy storage system. *International Journal of Hydrogen Energy*, 45(32):16239–16253, 2020.

[39] Chaima Mahjoubi, Jean-Christophe Olivier, Sondes Skander-Mustapha, Mohamed Machmoum, and Ilhem Slama-Belkhodja. An improved thermal control of open cathode proton exchange membrane fuel cell. *International Journal of Hydrogen Energy*, 44(22):11332–11345, 2019.

[40] Trevor Hocksun Kwan, Xiaofeng Wu, and Qinghe Yao. Bidirectional operation of the thermoelectric device for active temperature control of fuel cells. *Applied Energy*, 222:410–422, 2018.

[41] Fabio Musio, Fausto Tacchi, Luca Omati, Paola Gallo Stampino, Giovanni Dotelli, Stefano Limonta, Davide Brivio, and Paolo Grassini. Pemfc system simulation in matlab-simulink® environment. *International Journal of Hydrogen Energy*, 36(13):8045–8052, 2011.

[42] Maaspaliza Azri, Ayu Nurfatika Abdul Mubin, Zulkifilie Ibrahim, NA Rahim, and Siti Rohani Sheikh Raihan. Mathematical modelling for proton exchange membrane fuel cell (pemfc). *Journal of Theoretical and Applied Information Technology*, 86(3):409–419, 2016.

[43] F. M. White. *Fluid Mechanics. 7th Ed.* McGraw-Hill, 2011.

[44] Yunus A Cengel and A Ghajar. Heat and mass transfer (a practical approach, si version). *McGraw-670 Hill Education*, 671:52, 2011.

[45] John W Mitchell and James E Braun. *Principles of heating, ventilation, and air conditioning in buildings*. John Wiley & Sons, 2012.

[46] John H Lienhard. *A heat transfer textbook*. Phlogistron, 2005.

[47] Reza Omrani. Gas diffusion layer for proton exchange membrane fuel cells. In *PEM Fuel Cells*, pages 91–122. Elsevier, 2022.

[48] L Cindrella, Arunachala Mada Kannan, JF Lin, K Saminathan, Y Ho, CW Lin, and JJJOPS Wertz. Gas diffusion layer for proton exchange membrane fuel cells—a review. *Journal of Power Sources*, 194(1):146–160, 2009.

[49] Sang Youp Hwang, Han-Ik Joh, M Aulice Scibioh, Sang-Yeop Lee, Soo-Kil Kim, Tai Gyu Lee, and Heung Yong Ha. Impact of cathode channel depth on performance of direct methanol fuel cells. *Journal of Power Sources*, 183(1):226–231, 2008.

[50] Mohammad Ziauddin Chowdhury, Omer Genc, and Serkan Toros. Numerical optimization of channel to land width ratio for pem fuel cell. *International Journal of Hydrogen Energy*, 43(23):10798–10809, 2018.

[51] A Syampurwadi, H Onggo, R Yudianti, et al. Performance of pem fuel cells stack as affected by number of cell and gas flow-rate. In *IOP conference series: earth and environmental science*, volume 60, page 012029. IOP Publishing, 2017.

[52] Gaihua Wang, Qianyu Zhai, and Hong Liu. Cross self-attention network for 3d point cloud. *Knowledge-Based Systems*, 247:108769, 2022.

[53] Ebrahim Afshari, Nabi Jahantigh, and Masoud Ziaei-Rad. Parametric study of the influence of cooling channel dimensions on pem fuel cell thermal performance. *Iranian Journal of Hydrogen & Fuel Cell*, 4(4):265–274, 2018.

[54] Gary Sandrock. A panoramic overview of hydrogen storage alloys from a gas reaction point of view. *Journal of alloys and compounds*, 293:877–888, 1999.

[55] Fusheng Yang, Xiangyu Meng, Jianqiang Deng, Yuqi Wang, and Zaoxiao Zhang. Identifying heat and mass transfer characteristics of metal hydride reactor during adsorption: improved formulation about parameter analysis. *international journal of hydrogen energy*, 34(4):1852–1861, 2009.

[56] Shahrzad S Mohammadshahi, Tim Gould, Evan MacA Gray, and Colin J Webb. An improved model for metal-hydrogen storage tanks–part 1: Model development. *International Journal of Hydrogen Energy*, 41(5):3537–3550, 2016.

[57] Yan Shi, Holger Janßen, and Werner Lehnert. A transient behavior study of polymer electrolyte fuel cells with cyclic current profiles. *Energies*, 12(12):2370, 2019.

[58] Rupak Banerjee and Satish G Kandlikar. Two-phase flow and thermal transients in proton exchange membrane fuel cells–a critical review. *International journal of hydrogen energy*, 40(10):3990–4010, 2015.